

Big Rock and Streeter Creeks Base Flow Analysis

A Pilot Study for the Tenmile Creek Watershed, 2020

Brian P Murphy and Edward A Davis

Thomas Gast & Associates Environmental Consultants | 791 8th St. Suite H, Arcata, CA 95521

Table of Contents

| | |
|--|------------|
| Table of Tables | ii |
| Table of Figures | iii |
| Executive Summary | 1 |
| Introduction | 4 |
| Motivation | 4 |
| Study Site Background | 4 |
| Abiotic Factors | 7 |
| Climate | 7 |
| Anthropogenic Climate Change | 10 |
| Spatial Variation and Topographic Effects | 11 |
| Geologic Setting and Critical Zone Architecture | 13 |
| Biotic Factors | 15 |
| Biomass and Forest Composition..... | 15 |
| Anthropogenic Disturbances | 18 |
| Agriculture | 18 |
| Diversions..... | 20 |
| Legacy impacts of Timber industry | 21 |
| Fire Regime | 22 |
| Elder Creek Streamflow | 23 |
| Methods | 24 |
| Drainage Area Ratio | 24 |
| VELMA | 25 |
| Deficit Calculations | 26 |
| Simulated Historic Conditions | 26 |
| Results | 28 |
| Drainage Area Ratio | 28 |
| VELMA | 28 |
| Elder Creek Calibration | 28 |
| Big Rock Creek and Streeter Creek | 30 |
| Summer Streamflow Deficits | 33 |
| Deficits under Percent-of-Flow Diversions | 36 |

Historic Evapotranspiration37
References..... 38

Table of Tables

Table 1. Watershed areas 5
 Table 2. The slope of watersheds at 10m pixel resolution 12
 Table 3. Watershed relief at 30m pixel resolution. Watershed relief is calculated by subtracting the minimum elevation from the maximum elevation in the basin. 13
 Table 4. Cover types present in each watershed by percentage..... 15
 Table 5. Average biomass density in tons per acre (tons/acre) of Elder, Streeter, and Big Rock Creek watersheds..... 17
 Table 6. Comparison of the diversion ponds of Streeter and Big Rock Creeks..... 20
 Table 7. Parameters used in drainage area ratio calculations..... 24
 Table 8. Some required VELMA data inputs and sources used 25
 Table 9. Simulated old-growth spatial statistics in Big Rock Cr. and Streeter Cr..... 27
 Table 10. Summer season water deficits in Big Rock Cr. and Streeter Cr..... 34
 Table 11. Changes in modeled evapotranspiration (AET) with old-growth cover modifications..... 37
 Table 12. Modeled yields in Big Rock Cr. and Streeter Cr. with old-growth cover modifications..... 38

Table of Figures

Figure 1. To the left is a map of the Eel River watershed in relation to the state of California. To the right is a map of the sub-basins that drain the Big Rock and Streeter watersheds. These basins drain into the Tenmile Creek watershed, which is a major contributor to the South Fork Eel River watershed. 4

Figure 2. The elevation map of the study area. The highest point of elevation is Cahto Peak at 4216 ft tall, which divides Big Rock and Streeter Creek basins from the Elder Creek basin..... 6

Figure 3. Average monthly rainfall for Laytonville, California. The solid line is the average daily rainfall, while the (Weatherspark 2020) 7

Figure 4. Oceanic El Niño Index (ONI) based on a 3-month average from 1950 to 2016. Any year with an ONI value greater than 0.5 is considered to be in an El Niño event. Any year with an ONI of less than -0.5 is considered to be in a La Niña event. From Trenberth, 2016..... 9

Figure 5. The Elder Creek stream flow record between 1982 and 2018 (USGS Gage 11475560). Water Year types are listed on the y-axis. 9

Figure 6. Slope intensity map of the study site. Elder is uniformly steep, whereas Streeter and Big Rock are primarily steep only in the headwaters..... 12

Figure 7. Schematic cross-section of critical zone structure in the two main geologic units found in the Tenmile Creek study area, highlighting the difference in runoff processes. Not to scale. From Hahm et al. (2019)..... 14

Figure 8. Comparison of geological attributes of the Elder, Streeter, and Big Rock Creek watersheds. The map to the left shows the distribution of geo units. These two geologic belts are separated by the Coastal Belt Thrust, which has created a pattern in soil texture and soil depth further revealed in the map on the right. 15

Figure 9. Map showing the land cover classification of the region. Evergreen forest dominates Elder Creek, with smaller areas of hardwood trees and mixed tree stands. Streeter and Big Rock display a far more mixed mosaic of land cover types due to human disturbance and differences in the geology and soil..... 16

Figure 10. Forest attributes of Elder, Streeter, and Big Rock Creek watersheds. The differences in forest distribution and density are a result of both current and historic human land use as well as the underlying geology. These attributes affect how water interacts with the landscape. 17

Figure 11. Comparison of the forests of Big Rock, Streeter, and Elder Creeks from LEMMA’s gradient nearest neighbor (G.N.N.) dataset. These plots show the distribution of forest characteristics within the three watersheds. The high variability of the Big Rock forest reflects the impaired nature of the watershed and is evident when compared with the forest characteristics of the less impaired Streeter Creek and the unimpaired Elder Creek..... 18

Figure 12. The left map shows biomass density of the forests of Elder, Streeter, and Big Rock Creek watersheds as of 2012. The right map shows the change in biomass from 1990 to 2012 in tons per acre.

The inset map with NAIP imagery is a zoom in on the vineyards and retention ponds that replaced the forest. Ground-level images of these ponds can be seen in Figure 13..... 19

Figure 13. Comparison of the ponds in Streeter and Big Rock Creeks. Big Rock Creek watershed’s ponds are far larger and deeper than the ponds of Streeter Creek watershed. These maps show the presence of the ponds from 2012 to 2016 using manual digitization. The areas and volumes of these ponds are detailed in Table 5..... 21

Figure 14. Raster plot of Elder Creek (USGS 11475560) streamflow from 1 Jan 1982 – 31 Dec 2019 on a logarithmic scale. 23

Figure 15. Quantile-quantile plot of modeled and observed streamflow values in Big Rock Creek and Streeter Creek. All values are in cubic feet per second. 28

Figure 16. Goodness-of-fit metrics from final Elder Creek VELMA calibration. Dashed lines represent threshold values (logNSE = 0.9; NSE = 0.6). 29

Figure 17. Comparison of modeled and gauged summer recession limb streamflow in Elder Creek, 2018. 30

Figure 18. Quantile-quantile plot of modeled and observed discharges in Big Rock and Streeter Creek using VELMA. The dashed line represents a 1:1 ratio between modeled and observed values..... 30

Figure 19. Raster plot for VELMA modeled streamflow in Big Rock Creek. 31

Figure 20. Raster plot of VELMA modeled streamflow in Streeter Creek. 32

Figure 21. Summer 2018 recession hydrographs of BRL and SCL, comparing observed and modeled values 33

Figure 22. Summer 2019 recession hydrographs of BRL and SCL, comparing observed and modeled values 34

Figure 23. Daily streamflow deficits in Big Rock Creek as calculated under three baseline conditions: (1) VELMA modeled flow, (2) VELMA modeled flow with 10% subtracted, (3) VELMA modeled flow with 20% subtracted..... 36

Figure 24. Daily streamflow deficits in Streeter Creek as calculated under three baseline conditions: (1) DAR modeled flow, (2) VELMA modeled flow, (3) VELMA modeled flow with 10% subtracted, (4) VELMA modeled flow with 20% subtracted..... 37

Executive Summary

This project focused on understanding the low flows in Tenmile Creek tributaries in Mendocino, California. Tenmile Creek is a major tributary to the South Fork Eel River and is historically habitat for Steelhead, Chinook, and Coho. Tenmile Creek is considered an impaired stream for multiple reasons including, one of the most impactful being, low flows, which are common in this region due to a variety of both abiotic and biotic natural factors as well as human-caused factors. For this pilot project, the Tenmile Creek sub-basins of Big Rock Creek and Streeter Creek were analyzed with the goal of understanding the magnitude of various factors play in maintaining streamflow. Elder Creek, an unimpaired watershed located west of Cahto peak, was used as a comparison to Big Rock and Streeter creeks. These creeks are highly vulnerable to low flow events that negatively impair ecosystem functionally. Endangered species, including the endangered Coho and Chinook salmon, and threatened Steelhead are directly impacted by low summer flows in this area, by reducing habitat and creating conditions adverse for spawning. The four principals of river restoration that we use to guide this study are: (1) Flow determines physical habitat, which in turn determines the biotic composition, (2) maintaining natural patterns of connectivity (along the river and the floodplain) is essential for riverine species viability, (3) life histories of aquatic species have evolved in response to natural variations in stream condition throughout the year, and between wet and dry years, (4) regulation of flow regimes facilitates the invasion and success of introduced/exotic species, especially the loss of natural wet/dry cycles.

The largest driver of the streamflow is the amount of precipitation that the watershed receives. Precipitation is dictated by the climatic conditions, which exhibit large amounts of variability on a seasonal level, as well as an interdecadal level. This region is defined as having a Mediterranean climate due to its hot, dry summers and wet winters. In Laytonville, the average December precipitation amount is 10.5 inches of rain. This is in stark contrast to the average July precipitation amount of 0.1 inches of rain. On an interdecadal scale, this region experiences multiple phenomena, which can lead to extreme weather conditions. El Nino Southern Oscillation (ENSO) is one of the strongest interdecadal climate phenomena that arise as a result of shifting ocean surface temperatures in the Pacific Ocean. El Nino increases precipitation during winter and spring months. These events have been associated with some of the wettest years in this region in the last 40 years, including the wet seasons of 1981-1982, 1997-1998, and 2015-2016. The alternate variation of the ENSO cycle is La Nina, which typically lasts twice as long, and brings reduced fall temperatures, but increased temperatures and precipitation in the winter and spring. There is another climate phenomenon called the Pacific Decadal Oscillation (PDO), which transitions between cold and warm cycles every 20 - 30 years. ENSO and PDO transitions can coincide, increasing the intensity of extreme climate transitions.

Anthropogenic climate change is anticipated to increase global temperature by an average of 0.36 °F per decade, resulting in a temperature increase of 2.7 °F by 2050 from pre-industrial levels. Warming temperatures will increase the water holding capacity of the air, resulting in increased evaporation, and stronger storm systems. Climate models agree that Earth will warm, but the impacts on precipitation are less clear. There is no consensus on whether the average precipitation will increase, but many models predict that the precipitation frequency is likely to decrease. It is also widely agreed that extreme precipitation events will become more frequent. Additionally, drastic transitions from drought to wet periods are expected to become more common, such as the precipitation variation between the 2012-2016 drought and the 2016-2017 heavy precipitation. This is problematic for summer flows because

more precipitation leaves the watershed in extreme rainfall because it becomes surface runoff, instead of percolating into the groundwater.

There are also topographic effects on climate that create variations of precipitation across the landscape. Mountains, such as the range to the west of Laytonville containing Cahto peak, force air to rise and lose moisture, creating increased precipitation on the windward slopes, but reduced precipitation on the leeward slopes. Additionally, terrain influences soil thickness and the amount of precipitation that can be retained in the soil column. Thin soils on the tops of ridges have less water holding capacity than the thicker soils at the base of the hillslopes. The Big Rock and Streeter basins are primarily steep in the headwaters, but more gently sloping downstream. This is in stark contrast with the Elder creek basin that is uniformly steep.

Big Rock Creek and Streeter Creek straddle the NW-SW trending Coastal Belt Thrust fault, leading to complex geologic conditions that have direct consequences for their watershed hydrology. The bedrock geology of the region can be broadly divided into two pieces: the Coastal Belt, a sandstone-argillite formation with high infiltration rates and subsurface moisture storage, and the Central Belt, a clayey, sheared metamorphic formation with low infiltration rates and high surface runoff. The headwaters of Big Rock and Streeter Creeks are underlain by rocks of the Coastal Belt, while the lower 50–60% of the watersheds are underlain by the Central Belt formations. Elder Creek lies entirely within the Coastal Belt lithologic region. These geologic complexities make direct comparisons between Elder Creek and Big Rock and Streeter Creeks difficult.

Climate, geography, and topography determine the types of biomes that are present across the landscape. The headwaters of the Big Rock and Streeter Creek basins are primarily conifer dominated, while downstream across the Coastal Belt Thrust fault, there is a more diverse mosaic of conifer forests, hardwood forests, mixed forests, grasslands, and shrublands. This is a result of both bedrock geology and human modification. In the Big Rock and Streeter basins, modern agriculture has created a high demand for water. These crops require more water as they progress through the growing season, putting further demand on these creeks during the summer. Cannabis and vineyard cultivation are prominent, and both contribute directly to the reduction in streamflows due to diversions and ponds. Big Rock is significantly impacted because of extensive vineyards and retention ponds.

Historic logging and fire suppression have also modified the ecosystem composition in unnatural ways. Clearcutting was previously implemented in these basins, resulting in the proliferation of dense stands of even-aged conifers such as Douglas fir. These dense stands require more water due to the increased canopy and stem density, resulting in less water being available for the streams because of increased evapotranspiration.

The fire regime has been modified by policies of fire suppression, building up dense forests with higher amounts of undergrowth. Prior to European colonization, these forests were partially managed by indigenous practices of introducing fire, creating low-intensity burns that would decrease stand density, and increase variation in habitat. Additionally, natural succession occurs after fire events, allowing for the proliferation of more shade-tolerant species with lower water demands. The modern practices of fire suppression have caused an increase in stand density and homogenous species composition. These stands are less resilient to disturbances such as pests and pathogens and are more susceptible to extreme fire events that lead to more significant tree mortality.

TGAEC used two models to estimate historical streamflow and establish an ecological baseline for Big Rock and Streeter Creeks: (1) a modified drainage-area ratio equation and (2) U.S. EPA Visualizing Ecosystem Land Management Assessments (VELMA) model. Both models were computed from 1982–2019.

The drainage-area ratio method uses a simple equation to estimate daily unimpaired streamflow in an ungauged basin of interest—multiplying the daily streamflow in a reference watershed by the ratio of the drainage areas in the basin of interest and the reference basin. TGAEC used a modified version of this equation in an attempt to account for lithologic differences between the Elder Creek watershed and the Big Rock Creek and Streeter Creek watersheds that change their runoff characteristics.

VELMA is a spatially distributed ecohydrology model designed to simulate changes in streamflow and forest biomass under different land use and disturbance conditions (e.g., timber harvest and wildfire). The model utilizes elevation, land use, soil type, precipitation, temperature, and tree age to simulate catchment runoff resulting from the chosen land use conditions. These simulations can be compared against observed flow measurements from existing stream gauges to assess model performance. After calibrating VELMA for performance in an adjacent unimpaired reference basin with an extended gauging record, TGAEC estimated historic and naturalized streamflow without surface water diversions in both study basins.

The two models performed similarly well compared to gauging observations made in 2018 and 2019. Modeled flows above 1.0 cfs tracked gauged flows with a nearly 1:1 fit. The models indicated flow impairment during low flow periods—modeled flow was 7–50% higher during the summer-fall dry season.

TGAEC compared gauged streamflow during the late spring and summer of 2018 and 2019 to the unimpaired flow estimated by each of the models. In both cases, TGAEC found significant streamflow deficits in 2018 and milder deficits in 2019. In 2018, the observed dry season yield (May–November) in Big Rock Creek was 60.93 million gallons less than the modeled unimpaired yield. During this same period, the yield Streeter Creek lacked 23.10 million gallons compared to modeled values. Comparing total summertime (May–October) yields in 2019, deficits were absent in Big Rock Creek, but Streeter Creek yielded 16.21 million gallons less than the unimpaired model.

To investigate the effects of clear-cut logging followed by long-term fire suppression in the watersheds of Big Rock Creek and Streeter Creek, TGAEC modified the spatial inputs of the VELMA model to approximate old-growth conditions in Douglas-fir stands, as well as increased grassland area in historic oak savannah present in the lower watersheds. A 30% reduction was made to the coniferous forest cover, and these areas were converted to a mix of grassland and chaparral shrubs. VELMA's evapotranspiration model is designed to reduce evapotranspiration with increasing tree age. Therefore, 25% of the coniferous forest was randomly selected and increased in age by 100–400 years.

With these changes, VELMA calculated evapotranspiration was reduced by approximately 11% over the 38-year modeling period. The reduction in water use by tree cover was translated into an increase in water yields in both watersheds: approximately 8% in Streeter Creek and approximately 9% in Big Rock Creek. These results indicate that under pre-European contact conditions, streamflow in both watersheds was likely higher and that selective thinning of Douglas-fir stands may serve to increase flows.

Introduction

Motivation

The four principles of river restoration are: (1) Flow determines physical habitat, which in turn determines the biotic composition, (2) maintaining natural patterns of connectivity (along the river and the floodplain) is essential for riverine species viability, (3) life histories of aquatic species have evolved in response to natural variations in stream condition throughout the year, and between wet and dry years, (4) regulation of flow regimes facilitates the invasion and success of introduced/exotic species, especially the loss of natural wet/dry cycles.

Study Site Background

The Tenmile Creek watershed is located around the city of Laytonville in Mendocino County, California. The 22.04-mile creek drains a 65.38 square mile basin into the South Fork Eel River. It is considered an impaired watershed due to low stream flows that have hurt riparian organisms, including federally listed endangered species. Additional water is diverted from the stream channels for consumption, agriculture, and to be stored in ponds, further reducing the water available for aquatic organisms. The historical logging of the region has had many impacts that are still being felt in the watershed, including the growth of dense mid-seral stage Douglas-fir stands, which require more water than thinner old-growth stands.

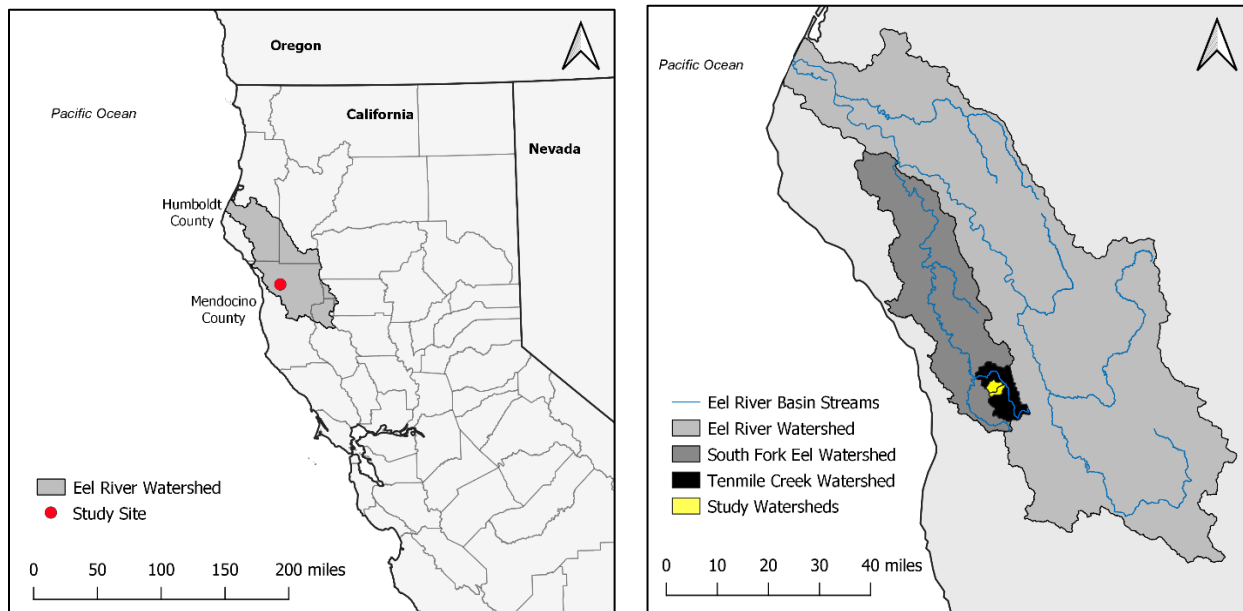


Figure 1. To the left is a map of the Eel River watershed in relation to the state of California. To the right is a map of the sub-basins that drain the Big Rock and Streeter watersheds. These basins drain into the Tenmile Creek watershed, which is a major contributor to the South Fork Eel River watershed.

In addition to low water levels and loss of stream connectivity, stream discharge is inversely proportional to stream heating, which results in reduced oxygen holding capacity, which further threatens Coho and chinook salmon (Stubblefield et al., 2012). Low-gradient streams are critical for Coho salmon rearing but are sensitive to low flow events that may cause stream dysconnectivity (Queener & Stubblefield, 2016). These species are a vital ecological, economic, and cultural resource to the Eel River watershed.

Table 1. Watershed areas

| Watershed Name | USGS Gauge No. | Area (mi²) | Area (acres) |
|-----------------------|-----------------------|------------------------------|---------------------|
| Elder Creek | 11475560 | 6.47 | 4143.95 |
| Streeter Creek | – | 4.85 | 3103.14 |
| Big Rock Creek | – | 2.98 | 1904.31 |

Before this project, there were no active gauges on Tenmile Creek, meaning that Streeter and Big Rock had no historical flow data, but there is a gauge on the nearby unimpaired Elder Creek. By comparing the impaired Tenmile Creek tributaries with the unimpaired Elder Creek, we can determine historical flows of Big Rock and Streeter Creeks to assess how land use and water diversion have impacted the stream flow. The combined area of Streeter and Big Rock basins is approximately equivalent to the area of the Elder Basin (Table 1).

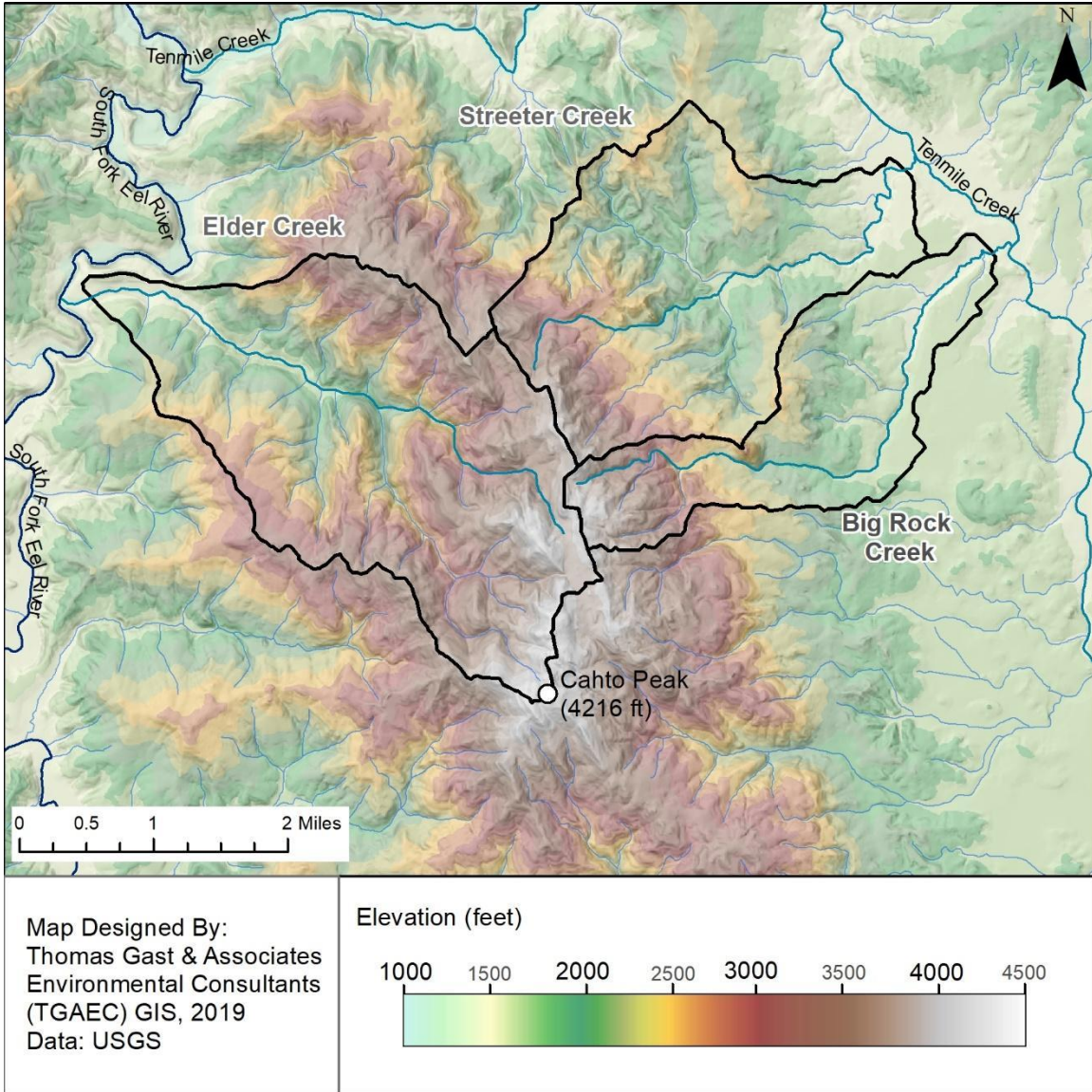


Figure 2. The elevation map of the study area. The highest point of elevation is Cahto Peak at 4216 ft tall, which divides Big Rock and Streeter Creek basins from the Elder Creek basin.

Abiotic Factors

Climate

This region is classified as having a Mediterranean climate because of its hot and dry summers and wet winters. The Mediterranean climate means that wet weather is primarily concentrated in just a few months out of the year in the winter months. Ultimately only a few major storm systems end up dictating the amount of precipitation that the watersheds receive during the short wet season. Storm systems are generated in the North Pacific between Hawaii and Alaska and move eastward into the west coast of North America along the jet stream. These storms take on characteristics of the regions in which they formed. Storms that originate from the Gulf of Alaska are colder and drier, while the storms that originate from the mid-Pacific and Hawaii are warmer and wetter (Mount, 1995). Because precipitation mainly comes in the winter months, followed by dry summers, streams in these climates are more susceptible to drying out when there are summer water withdrawals.

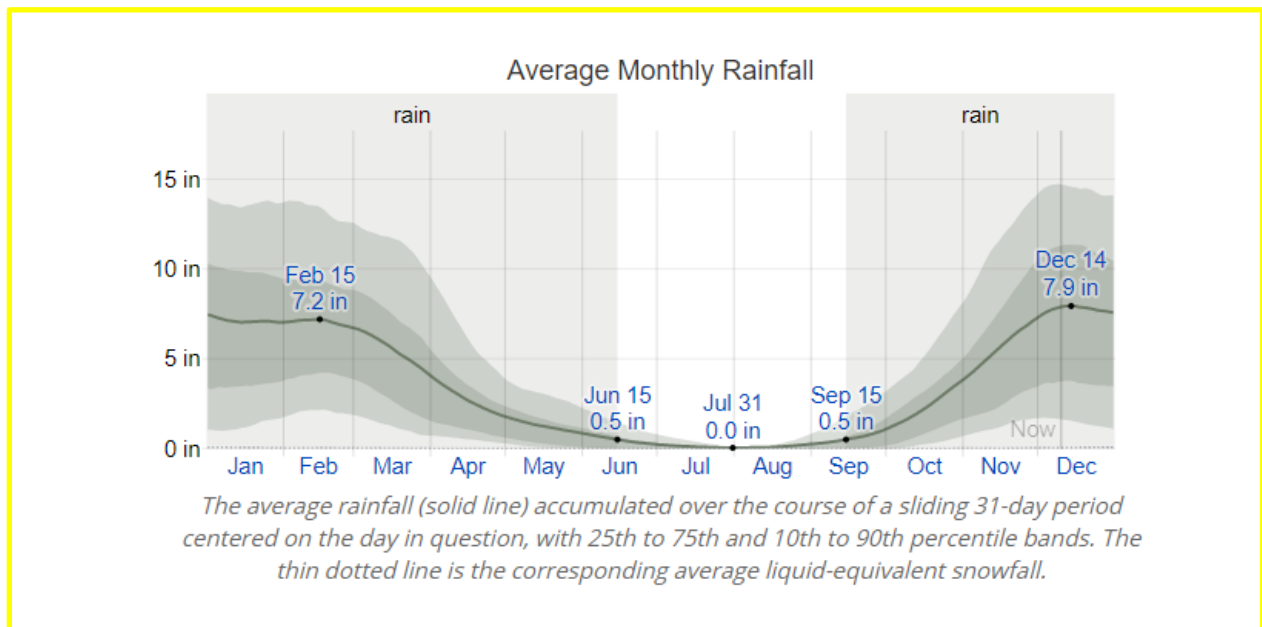


Figure 3. Average monthly rainfall for Laytonville, California. The solid line is the average daily rainfall, while the (Weatherspark 2020)

The climate of the region experiences dramatic variations in precipitation amounts on an annual basis. This variation can be seen in the oscillations between dry and wet years, where wet years receive almost three times as much precipitation as dry years (Figure 33). Periods of consecutive dry years are even more susceptible to ecosystem damaging low flow events.

The climate in California is determined by ocean currents and ocean surface temperature, which determine the movement and generation of the storms that hit Northern California. The temperature of the uppermost 1000 feet of the waters in the North Pacific influences the types of atmospheric pressure cells that are formed. Warm surface temperatures are correlated with the formation of stationary low-

pressure cells, while cooler surface temperatures are associated with high-pressure cells. The presence of these pressure cells dictates the direction that eastward storm systems take. High-pressure cells off the coast of California deflect storm systems away from the state and take them northward instead. Alternatively, low-pressure cells bring more storms from the Mid-Pacific and Alaska regions (Mount, 1995).

On a larger climactic scale, there are many cycles of ocean temperatures, currents, and atmospheric conditions that play a large role in dictating the climate. Two interdecadal climate phenomena can produce significant variations in climate in western North America (Jain et al., 2012). A historical climate record has been inferred based on 150 years of instrumental climate records, and 400 years of tree ring data (dendrochronology) (McGregor et al., 2010). Dendrochronology has been successfully used to predict high-resolution climate records in North America. These tree ring records show that there is decadal-scale variability of the climate (Biondi et al., 2001). The more temporary of the two is called the El Niño/Southern Oscillation (ENSO), which has two variations called El Niño and La Niña. El Niño events occur every 2 to 7 years and last for 9 to 12 months, bringing increased precipitation from winter to spring. This oscillation of atmospheric pressure moves between the West Indian Ocean and the Southern Pacific Ocean, creating a cascade of air pressure, ocean currents, and ocean temperature variations (McGregor et al., 2010). A consequence of this is a warm pool of water that originates in the equatorial regions of the Indian Ocean moves eastward across the Pacific due to weaker westerly trade winds, modifying the atmospheric river called the Jetstream, and increasing the monsoonal moisture that Northern California receives. Major El Niño events include the years of 1982-1983 and 1997-1998, and 2015-2016 (Figure 4)(Mount, 1995) (Cai et al., 2014a) (Santoso et al., 2017). La Niña events usually occur every 4 to 14 years for 1 to 3 years, bringing cooler temperatures in the fall, followed by increased temperature and precipitation in the winter and spring months (Jain et al., 2012). Multi-year El Niño events have been recorded multiple times over the last 350 years. There appears to be a statistically significant link between volcanic activity and the likelihood of an El Niño or La Niña event occurring the following year (McGregor et al., 2010).

The other prominent climate phenomenon that has been detected in the North Pacific is called the Pacific Decadal Oscillation (PDO), which oscillates between warm and cold cycles every 20 to 30 years. PDO patterns have been detected in rates of forest growth via dendrochronology in North America. Because sea surface temperature records have only existed since the beginning of the 1900s, these long-term low-frequency variations are challenging to assess (Biondi et al., 2001). The effects of an ENSO cycle can be impacted by the phase of the PDO (Jain et al., 2012). Dramatic climate transitions have been found when the ENSO and the PDO transition to opposite states at the same time (Biondi et al., 2001).

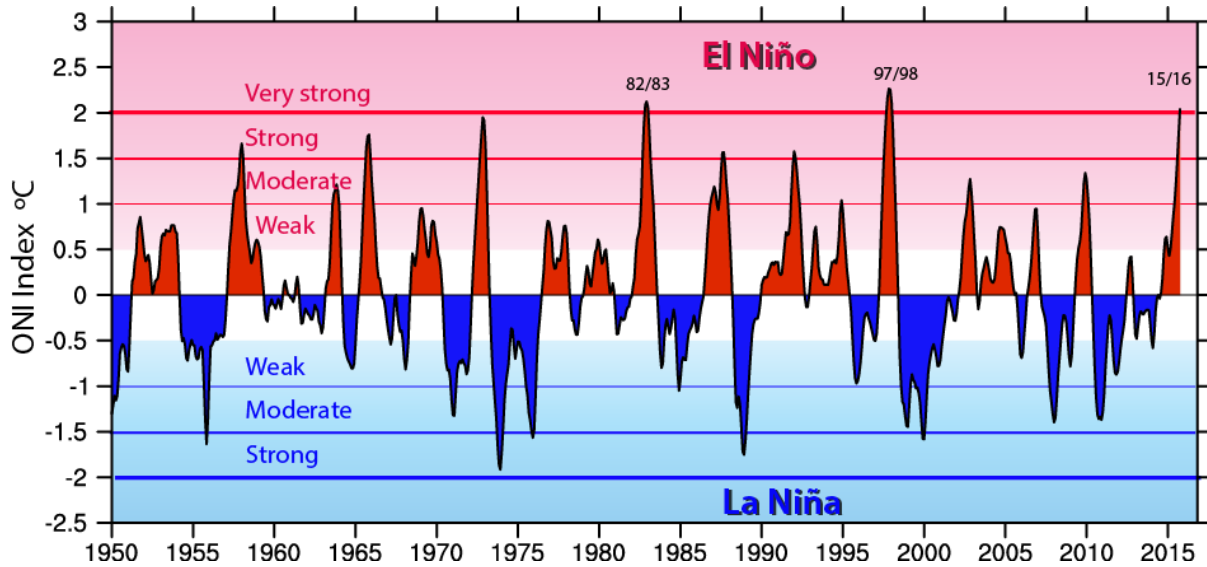


Figure 4. Oceanic El Niño Index (ONI) based on a 3-month average from 1950 to 2016. Any year with an ONI value greater than 0.5 is considered to be in an El Niño event. Any year with an ONI of less than -0.5 is considered to be in a La Niña event. From Trenberth, 2016.

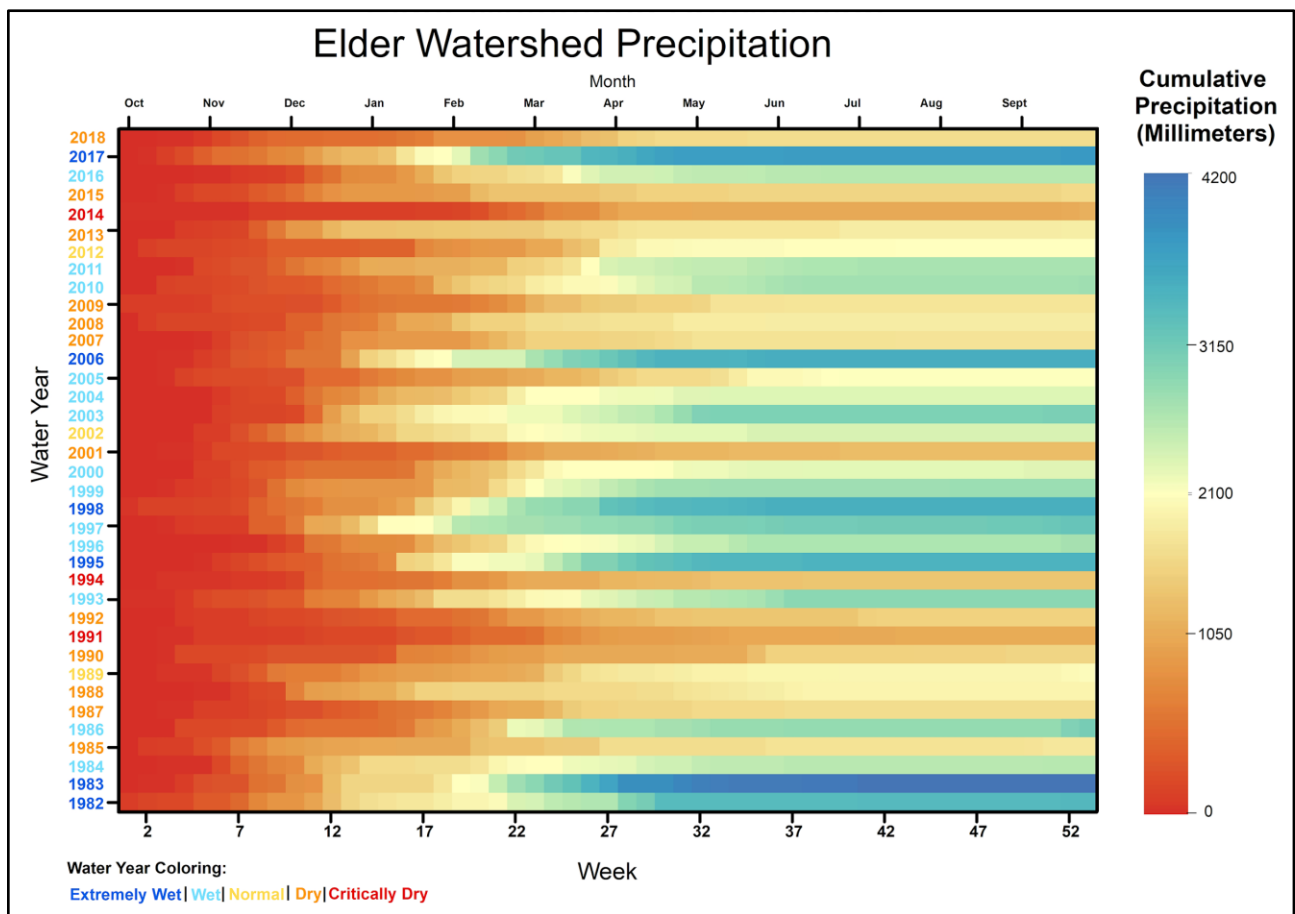


Figure 5. The Elder Creek stream flow record between 1982 and 2018 (USGS Gage 11475560). Water Year types are listed on the y-axis.

Anthropogenic Climate Change

Anthropogenic climate change is expected to have lasting impacts on the climate of Northern California. Our understanding of climate change is based on instrumental records from the past 150 years, and extensive tree ring records. Many climate models have been created to understand the potential impacts of natural climate fluctuations in conjunction with anthropogenic greenhouse gas induced climate change. These computer models unanimously predict that temperatures across the globe are widely predicted to increase under climate change (Berg & Hall, 2015). A global increase of 1.0 °C (1.8 °F) is estimated to have been caused by human activity in the last 150 years. Warming is expected to continue to 1.5 °C (2.7 °F) between 2030 to 2050. Warming is modeled to increase at a rate of 0.2 °C (0.36 °F) per decade due to past and current emissions (IPCC, 2018). These temperature increases will directly affect California by increasing evaporation rates and accelerating land surface drying. For every degree Celsius of temperature rise, the water-holding capacity of the air increases by 7%, increasing potential evapotranspiration. Globally, this is expected to increase warming at the equator, increasing the chances of atmospheric convection and storm occurrence (Cai et al., 2014b). In the Pacific Ocean, this increased air moisture creates stronger storm systems, leading to more significant precipitation events that will land on the west coast of North America (Trenberth, 2011) (Pierce et al., 2013).

Climate models agree that California's climate will warm, and extreme precipitation events are expected to increase, but the consensus of impacts on annual precipitation are less clear (Pierce et al., 2013). While there is no consensus among current climate models in regards to future net change mean total precipitation, it is widely predicted to the standard deviation of interannual precipitation totals will increase (Berg & Hall, 2015) (Pierce et al., 2013). Precipitation amounts and timing will become more erratic on a decade level. Northern California is projected to have the most significant increase in daily precipitation intensity compared to the rest of the state (Berg & Hall, 2015). Most models predict that that precipitation frequency will decrease by 6-14 days by 2060, but only half of the models predict that daily precipitation will increase, accounting for an average annual precipitation increase of 5.3% (Pierce et al., 2013). Winter mean precipitation is anticipated to increase, while spring precipitation and fall precipitation is expected to decrease (Swain et al., 2018). Anthropogenic climate change is also projected to modify the interdecadal ENSO cycle and increase the frequency of extreme El Nino events (Cai et al., 2014b). The shift from drought to extreme wet was caused by a large number of storms delivered by the atmospheric river associated with an El Nino event. Additionally, global warming is predicted to increase the frequency of persistent high-pressure ridges off the California coast (Swain et al., 2018).

In the context of the whole state, Northern California is expected to receive the most significant increase in heavy precipitation events as a result of anthropogenic climate change (Swain et al., 2018) (Pierce et al., 2013). All models indicate extreme dry wet season transitions are predicted to become 1.5 to 2 times more common, while wet extremes are predicted to triple in 2060-2100 compared with the historical climate record (Swain et al., 2018) (Berg & Hall, 2015). An example of an extreme dry wet season is the drought of 2012-2016, followed by an extremely wet period in 2016-2017 (Swain et al., 2018). By the end of the twenty-first-century, increases in extreme dry events are projected to increase

beyond natural climate variability (Berg & Hall, 2015). Additionally, extreme El Nino events, such as the ones that occur in 1982-1983, 1997-1998, and 2015-2016 can generate to larger atmospheric convection zones, increasing rainfall in the eastern Pacific (Cai et al., 2014b). Increased extreme rainfall events are detrimental to low flow events because they lead to greater runoff, which reduces the amount of soil absorption (Trenberth, 2011). Steady, consistent rainfall allows for more surface infiltration because of the soil has more time to drain. When saturated soil receives additional precipitation, it remains on the surface and drains into channels (Pierce et al., 2012). Higher surface runoff leads to greater streamflow during and directly after the precipitation event, but reduces the amount of soil water and groundwater that drives streamflow during the dry season. The combination of increasing temperature, evapotranspiration, and the seasonal disconnect between peak water inputs and peak water demand expected as a result of climate change will put substantially more pressure on summer low flow events (Stubblefield et al., 2012).

Spatial Variation and Topographic Effects

In addition to temporal variation, there is spatial precipitation variation within the watersheds due to the orographic effect. Orographic effects are changes in precipitation that are caused by terrain. As air rises over mountainous terrain, the atmospheric pressure increases, causing the air to release moisture, increasing precipitation. As this air mass moves to the other side of the mountain, it contains less moisture, releasing less precipitation, in a phenomenon called the rain shadow effect (Mount, 1995). In this region, the windward slopes are the west slopes. Elder lies on the west side of Cahto peak, while Streeter and Big Rock lie on the east side of Cahto peak, causing them to get less rainfall than Elder. There is an elevation difference of over 2500 feet between Cahto peak and the lowest points of all three watersheds.

Topography and slope of a basin influence how water travels through a watershed. Bedrock weathering rates are greater on steeper slopes, creating a more extensive hydrologically active layer in steeper basins than in valley bottoms where the critical zone is much thinner. Soils are thinnest along the ridges, and thickest at the base of the hillslopes, leading to more water retention. Steeper slopes and higher elevations correspond to greater summer flow, and slower flow recessions. Gentler slopes have been shown to increase the time required for water to pass through the basin. During regular flows, an upslope accumulated area (UAA) is a good predictor of when a hillslope is hydrologically connected to the stream system. During low flow events, the UAA has less of an influence on streamflow (Queener & Stubblefield, 2016).

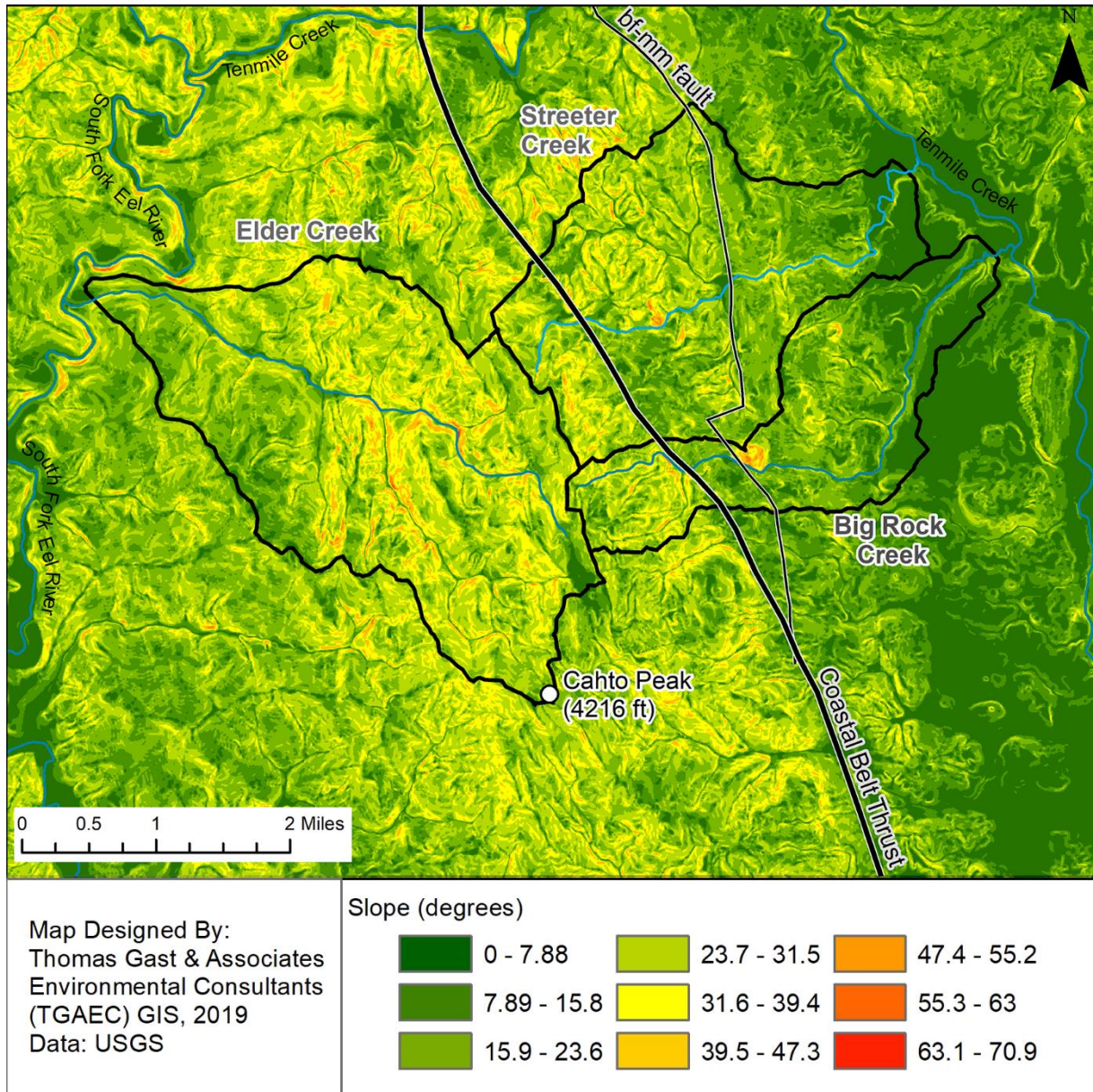


Figure 6. Slope intensity map of the study site. Elder is uniformly steep, whereas Streeter and Big Rock are primarily steep only in the headwaters.

Table 2. The slope of watersheds at 10m pixel resolution

| Watershed Name | Average slope (degrees) |
|----------------|-------------------------|
| Elder Creek | 25.45 |
| Streeter Creek | 20.59 |
| Big Rock Creek | 16.43 |

Table 3. Watershed relief at 30m pixel resolution. Watershed relief is calculated by subtracting the minimum elevation from the maximum elevation in the basin.

| Watershed Name | Watershed Relief |
|-----------------------|-------------------------|
| Elder Creek | 2807 ft |
| Streeter Creek | 2470 ft |
| Big Rock Creek | 2488 ft |

Geologic Setting and Critical Zone Architecture

The critical zone is the region between the top of the plant canopy and the elevation of chronically saturated, un-weathered bedrock (Dralle et al., 2018; Hahm et al., 2019; Salve et al., 2012). The architecture of the critical zone dictates how water is used, stored, and released within a landscape (Hahm et al., 2019). Because *in situ* formations of soil and saprolite (chemically weathered bedrock below the mobile soil layer) is dependent on the bedrock lithology, the identification of these units is crucial to our understanding of critical zone hydrology in our study area (Hahm et al., 2019; Salve et al., 2012).

As illustrated in Figure 8, the bedrock geology of the region is characterized by two belts of the Jurassic-Cretaceous aged Franciscan Complex—the Coastal Belt and the Central Belt—separated by the Coastal Belt Thrust fault (Jayko et al., 1989). Within the study area, the Coastal Belt is chiefly comprised of the Yager terrane—deeply weathered and steeply-dipping interbedded sandstone and argillite that is metamorphosed at the zeolite facies (Hahm et al., 2019; Jayko et al., 1989; McLaughlin et al., 2000). The Central Belt in our study area can be divided broadly into two formations that occur in fault contact with each other: the broken formation and mixed mélange (Jayko et al., 1989). The broken formation is similar in composition to the Yager terrane; however, its grains are more cemented, and it has undergone a slightly higher degree (pumpellyite) of metamorphism (Hahm et al., 2019; Jayko et al., 1989). The mixed mélange is composed of individual blocks of varying lithology (e.g., greenschist, greywacke, chert) in a highly sheared argillite-matrix (Hahm et al., 2019; Jayko et al., 1989). At the fault contact between the Coastal and Central Belts lies the Brush Mountain Shear zone, where rocks are generally composed of the sheared argillite of the mixed mélange (Jayko et al., 1989).

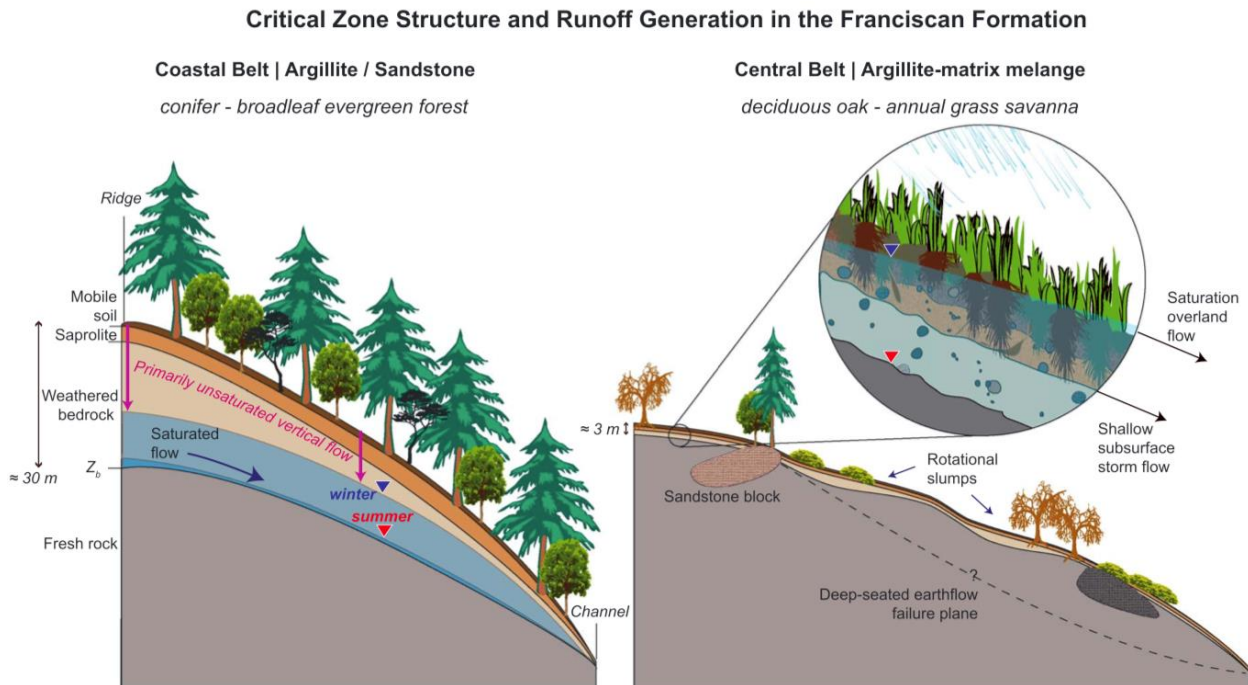


Figure 7. Schematic cross-section of critical zone structure in the two main geologic units found in the Tenmile Creek study area, highlighting the difference in runoff processes. Not to scale. From Hahm et al. (2019)

The deep weathering and fractured nature of the argillite-sandstone Yager terrane facilitate the storage of moisture in the subsurface, even though periods of extended drought conditions (Dralle et al., 2018; Hahm et al., 2019). Fractures in the weathered bedrock act as preferential pathways for moisture at the surface (e.g., rainfall) to make its way to greater depths before emerging at the surface as streamflow (Figure 7; Dralle et al., 2018; Hahm et al., 2019). These subsurface characteristics make the Yager terrane a “water-storing landscape” (Lovill et al., 2018). In contrast, the sheared and cemented character of the Central Belt *mélange* form a “water-shedding landscape,” due in part to its clayey composition (Figure 8; Lovill et al., 2018). These clays swell as the soil and saprolite become saturated, closing off any fractures or preferential pathways that may have been present (Lovill et al., 2018). As stated before, the “broken formation” of Jayko et al. (1989) is similar to the Yager terrane, but its cementation likely leads to a lower subsurface storage capacity.

The natural differences in lithology that determine subsurface moisture storage also determine the characteristics of baseflow—streamflow that occurs due to release of deeper subsurface moisture from surrounding hillslopes rather than runoff generated during storm events (Dralle et al., 2018; Hahm et al., 2019; Lovill et al., 2018). We expect that Elder Creek will have a greater baseflow discharge than Big Rock or Streeter Creeks relative to its size due to lying within the Yager terrane. Likewise, we expect Streeter Creek to have a greater baseflow than Big Rock Creek because it has a smaller fractional area underlain by Central Belt *mélange*.

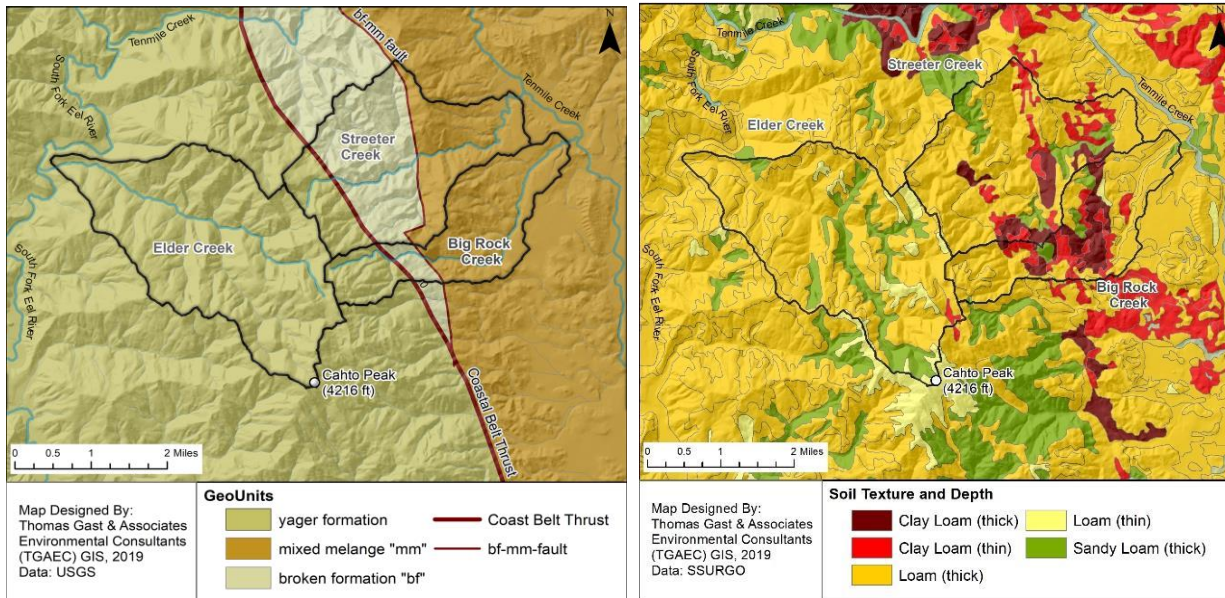


Figure 8. Comparison of geological attributes of the Elder, Streeter, and Big Rock Creek watersheds. The map to the left shows the distribution of geo units. These two geologic belts are separated by the Coastal Belt Thrust, which has created a pattern in soil texture and soil depth further revealed in the map on the right.

Biotic Factors

Biomass and Forest Composition

Elder and the headwaters of Streeter and Big Rock creeks are conifer dominated forests. The primary species is Douglas fir. There are small stands of shrubs and mixed coniferous, and hardwood stands interspersed throughout, especially on higher elevation ridges, and in the human-influenced land. There is a distinct difference in vegetation on the west side of the thrust fault where the underlying geo units change from Yager formation to mixed mélange. This division of geo units corresponds with a change in land cover and land use. On the west of the fault, the land cover is much more diverse. In the forests specifically, there is much more significant variation, with stands of mixed forests and pure hardwoods interspersed within stands of conifers.

Table 4. Cover types present in each watershed by percentage

| Cover type | Elder Creek | Streeter Creek | Big Rock Creek |
|----------------|-------------|----------------|----------------|
| Conifer | 93.3% | 58.1% | 53.9% |
| Grass | 0.2% | 8.4% | 11.3% |
| Bare Earth | 1.6% | 7.6% | 7.2% |
| Hardwood / Oak | 2.2% | 8.8% | 6.0% |
| Shrub | 2.2% | 12.3% | 15.0% |
| Mixed Forest | 0.5% | 5.0% | 6.6% |

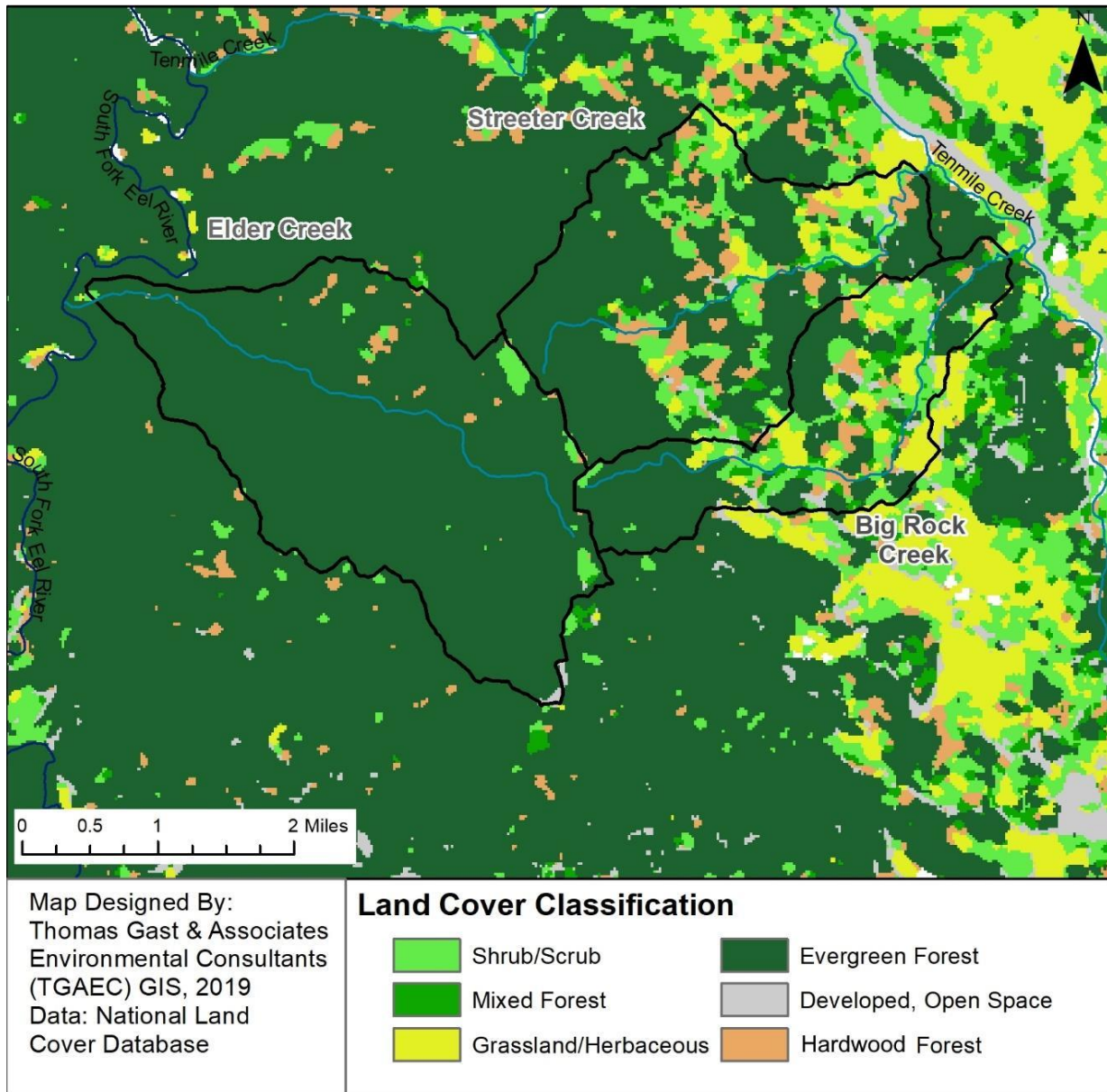


Figure 9. Map showing the land cover classification of the region. Evergreen forest dominates Elder Creek, with smaller areas of hardwood trees and mixed tree stands. Streeter and Big Rock display a far more mixed mosaic of land cover types due to human disturbance and differences in the geology and soil.

In Douglas-firs, strong relationships exist between seasonal water use and basal area, diameter breast height (DBH), and sapwood basal area. Young stands have a greater sapwood area per unit basal area, as well as a greater sap flux density, resulting in greater water use by the stand than a mature stand with the same area (Moore et al., 2004). Water use by the trees linearly decreases as the number of trees decreases. Additionally, water use decreases as the canopy closes up, and suppressed trees die out, lowering stand density (Stubblefield et al., 2012). Tree age has been determined to have a substantial influence on water use, with young trees having an average sap flux density 2.3 times higher in than in old-growth Douglas firs. Douglas fir roots grow deeper as it transitions from a younger tree to a mid-

seral stage tree, allowing them to access deeper water in the soil column. Additionally, the basal area of the stand was found to have a significant impact on the stand’s water use. Mature trees consume less water per sapwood area or unit leaf area than mid-seral stage trees (Moore et al., 2004). There are two distinct areas within the both of the study basins that demonstrate the highest values of basal area and percent canopy: the forests in the western headwaters and the forests on the far east of the basins, near the confluences with Tenmile creek (Figure 10). As succession continues and the age of the trees increases, changes in structure and composition occur, leading to the emergence of plants that are more tolerant to shade in the understory of the stand. These shade-tolerant species are more abundant in old-growth forests and where they consume less water per unit sapwood area than shade-intolerant species. According to sap flow measurements conducted in western Oregon, young Douglas-fir stands in riparian areas had 3.27 times higher water usage than old-growth stands during summer months (Moore et al. 2004). This period coincides with the dry season in the Tenmile Creek basin when water resources are in high demand by humans.

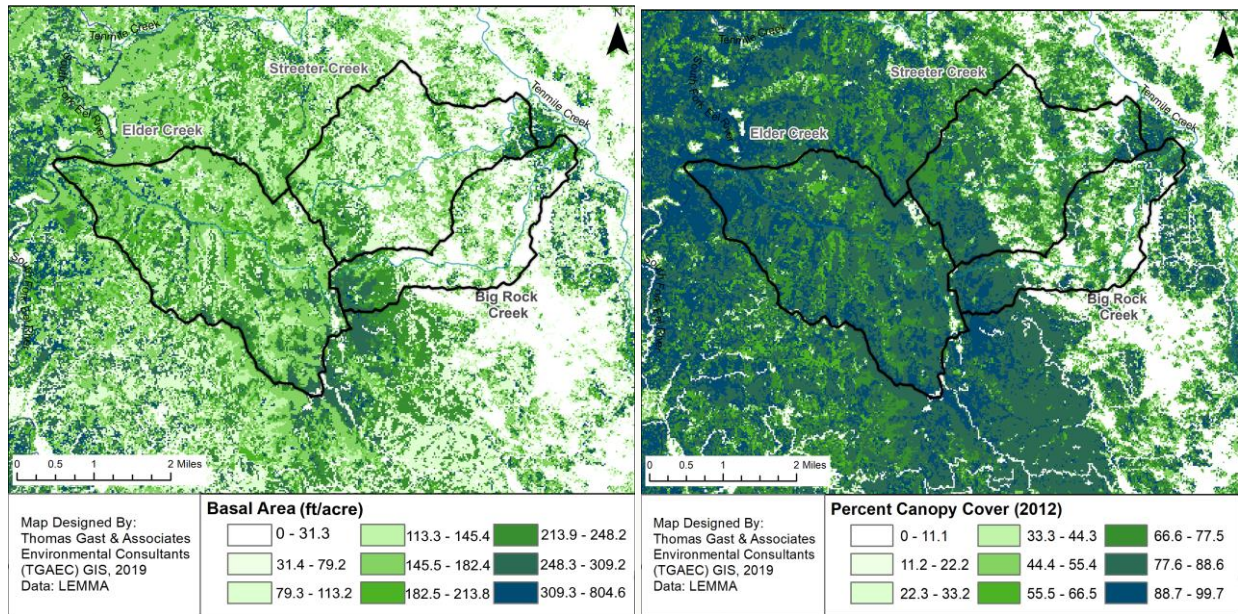


Figure 10. Forest attributes of Elder, Streeter, and Big Rock Creek watersheds. The differences in forest distribution and density are a result of both current and historic human land use as well as the underlying geology. These attributes affect how water interacts with the landscape.

Table 5. Average biomass density in tons per acre (tons/acre) of Elder, Streeter, and Big Rock Creek watersheds.

| Watershed | Mean | Standard Deviation |
|----------------|----------|--------------------|
| Elder Creek | 54.40064 | 9.30097 |
| Streeter Creek | 41.09378 | 19.6904 |
| Big Rock Creek | 36.24925 | 21.30078 |

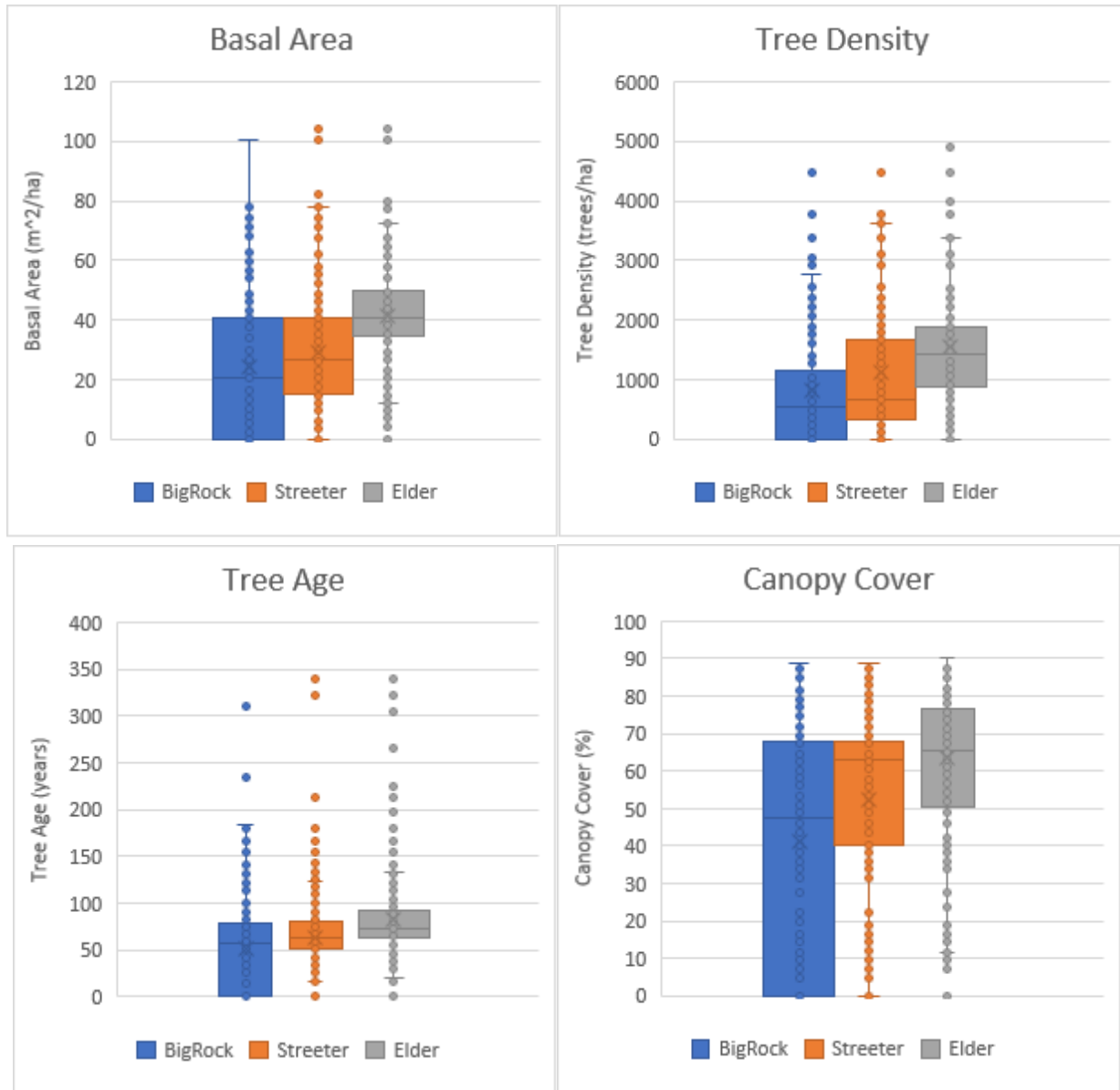


Figure 11. Comparison of the forests of Big Rock, Streeter, and Elder Creeks from LEMMA’s gradient nearest neighbor (G.N.N.) dataset. These plots show the distribution of forest characteristics within the three watersheds. The high variability of the Big Rock forest reflects the impaired nature of the watershed and is evident when compared with the forest characteristics of the less impaired Streeter Creek and the unimpaired Elder Creek.

Anthropogenic Disturbances

Agriculture

Water abstractions for agriculture are a significant contributor to low stream flow in these impaired watersheds. Steelhead trout and Chinook salmon are both native species that are susceptible to adult and juvenile mortality low stream flow (Bauer et al., 2015; Butsic & Brenner, 2016). As streamflow decreases, the temperature of the water rises and holds less oxygen, reducing or destroying spawning

Big Rock and Streeter Creeks Base Flow Analysis

habitat. In the past few years, Tenmile creek has had significantly reduced flows that prohibited the spawning of salmon in these streams and led to fish die-offs. In 2018, Big Rock Creek went completely dry in the summer. These basins contain intensive cannabis and wine agriculture. Each of these crops has different physical requirements that affect how they are grown. The social perceptions of these crops impact the spatial distributions of their impacts. These crops require irrigation and land to be cleared of native vegetation, both processes that modify the hydrological regime of the region. The most abrupt changes in biomass to occur in the west Tenmile basin in the 32 years between 1990 and 2012 are related to the deforestation caused by the creation of vineyards in the headwaters of the Big Rock Creek and Mud Springs Creek to the southeast. The creation of the retention ponds and the vineyards caused the removal of 1350 tons of biomass from the Tenmile Creek watershed (Figure 12). This region stands in contrast with the surrounding areas of the west Tenmile Creek watershed because it is one of the only places that is seeing a cluster of prominent biomass decrease. This number was derived from calculating the difference between the 1990 and 2012 LEMMA GNN biomass rasters. The 25.5-acre area of significant loss within the vineyard property was isolated and statistical analysis was performed. The average loss in this area was 53.0 tons per acre, with peak losses reaching up to 180 tons per acre.

As of 2014, there were 52 grows within Big Rock and Streeter Creek watersheds. These grows took up a total area of 8.6 acres, with an average biomass loss of 2.36 tons per acre, and an overall loss of 20.29 tons of biomass. Not only is there less deforestation associated with the cannabis grows, but it is also far more spread out across the landscape than the vineyards.

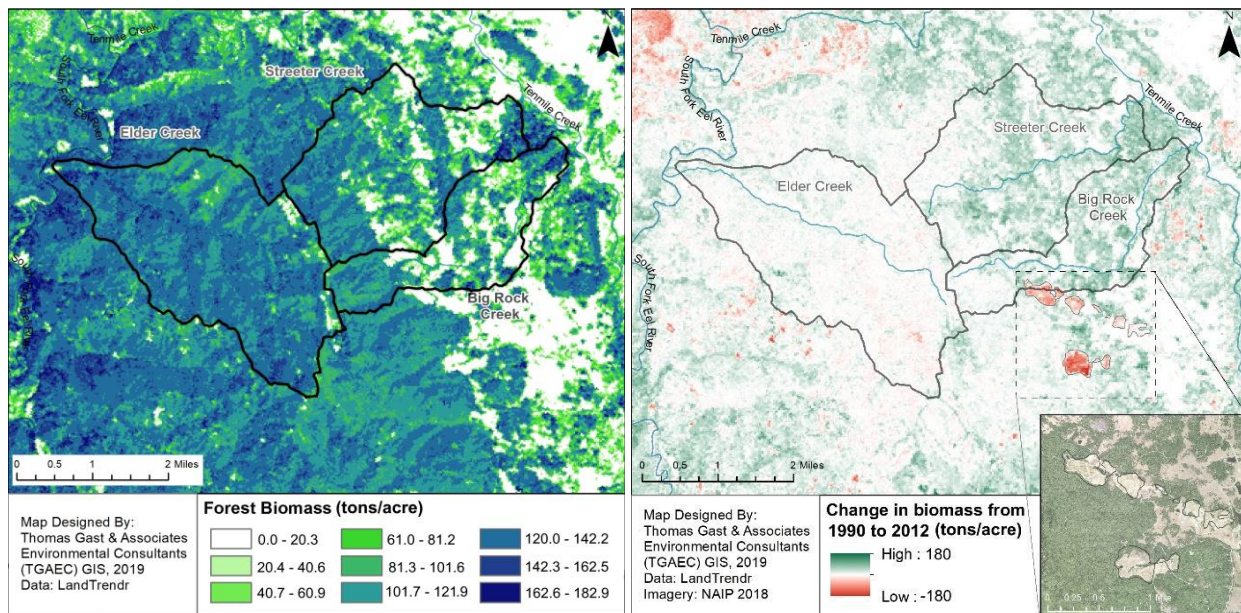


Figure 12. The left map shows biomass density of the forests of Elder, Streeter, and Big Rock Creek watersheds as of 2012. The right map shows the change in biomass from 1990 to 2012 in tons per acre. The inset map with NAIP imagery is a zoom in on the vineyards and retention ponds that replaced the forest. Ground-level images of these ponds can be seen in Figure 13.

Diversions

Small surface water diversions are the primary source for domestic and agricultural water in Northern California. These diversions are required to be registered with the State Water Resources (SWRCB), but Bauer et al. have found that there were lower numbers of registered diversions than there were grow sites, implying there is less compliance among the cannabis growing community (Bauer et al., 2015). Federally illegal status makes growers less likely to comply with the water management permitting requirements. The footprint of these grows small compared to the footprint of other agriculture commodities in California, but their distribution contributes to their environmental harm (Butsic & Brenner, 2016). Cannabis grows tend to be unevenly distributed and clustered together, meaning their impacts can be cumulative. In the Streeter and Big Rock watersheds, approximately 70% of the grows are within a 500-foot radius of a creek. The average water use of a cannabis plant is around 22.7 liters (6 gallons) per plant per day over the 150-day growing season (Humboldt Growers Association, 2011). These figures do not account for inefficiently designed and implemented water infrastructure on any of these unregulated grow sites, which could be extracting more water than is required for the crop (Bauer et al., 2015). Operation of several standard-sized pumps operating at 38 liters per minute could dewater the stream if the flow is already low enough, leaving these small headwater streams especially susceptible during the summer season. Both grapes and cannabis have a greater water demand as the plants grow, putting more stress on low flowing summer streams (Bauer et al., 2015).

The water requirement for a grapevine is around 12.64 liters (3.3 gallons) per plant per day, almost half of what a cannabis plant requires (Williams, 2001). The production of a single 125mL glass of wine requires the input of 120 liters of water (Hoekstra & Chapagain, 2006). For comparison, an average Northern Californian household uses approximately 650 liters per day for indoor domestic use (DeOreo, 2011). Unlike the cannabis grows in these watersheds, the vineyards are concentrated and sprawling. The retention ponds are more extensive and are filled with pumped groundwater as well as surface runoff. The series ponds of the around vineyard in upper Big Rock and Mud Creeks are notable because they are consecutive and drain water from the headwaters of Big Rock Creek (Figure 13).

Table 6. Comparison of the diversion ponds of Streeter and Big Rock Creeks

| Big Rock Creek | Count | Area (acres) | Estimated volume (acre-feet) |
|-----------------------|--------------|---------------------|-------------------------------------|
| 2012 | 5 | 3.776 | 14.233 |
| 2014 | 5 | 3.076 | 11.909 |
| 2016 | 5 | 3.641 | 14.074 |
| Streeter Creek | Count | Area (acres) | Estimated volume (acre-feet) |
| 2012 | 5 | 0.721 | 1.534 |
| 2014 | 6 | 0.664 | 1.311 |
| 2016 | 7 | 0.779 | 1.621 |

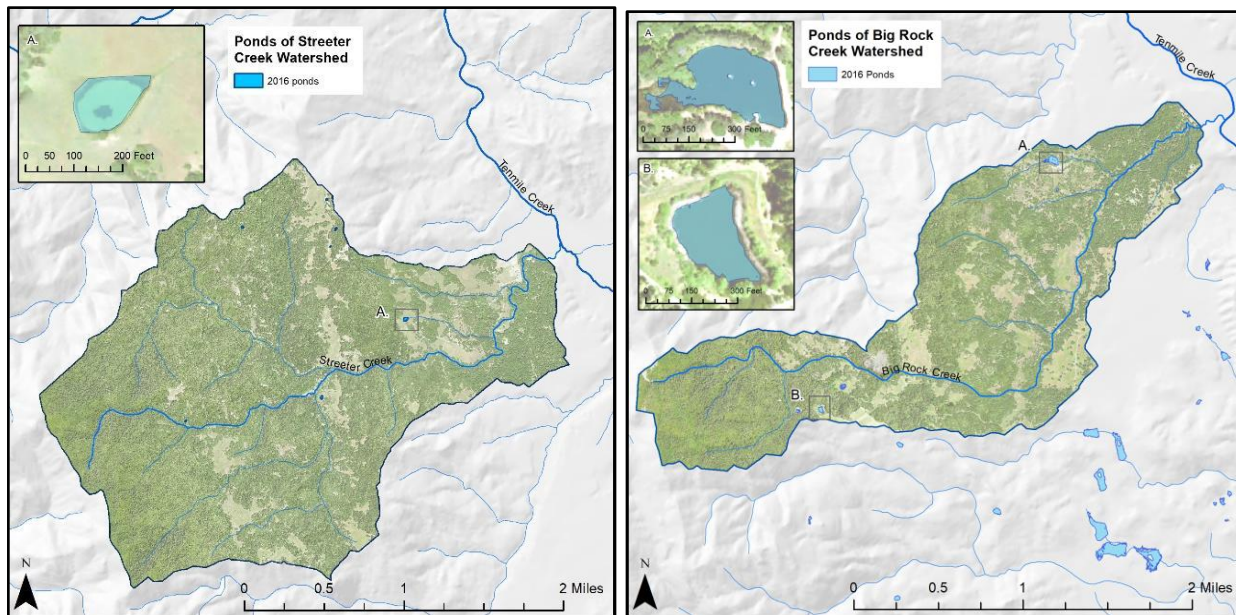


Figure 13. Comparison of the ponds in Streeter and Big Rock Creeks. Big Rock Creek watershed's ponds are far larger and deeper than the ponds of Streeter Creek watershed. These maps show the presence of the ponds from 2012 to 2016 using manual digitization. The areas and volumes of these ponds are detailed in Table 6.

Legacy impacts of Timber industry

Tree water use varies with tree age, size, and density. Tree water use is strongly correlated with tree size measurements such as basal area, diameter, and sapwood area (Stubblefield et al., 2012). Water use can be determined by amounts of transpiration, which can be measured by sap flow (Stubblefield et al., 2012). Transpiration rates and events are determined by multiple external factors such as vapor pressure deficit, temperature, and humidity, as well as stand specific factors such as species composition, sapwood basal area, stand age, and stand density (Queener & Stubblefield, 2016). Conifers and broadleaf evergreen trees rely on water from different portions of the regolith and have a peak water use at different times of the year. Douglas fir water use peaks during the spring while water is most available, while broadleaf evergreens, such as madrone, transpire greatest during late summer (Queener & Stubblefield, 2016).

In Douglas-firs, strong relationships exist between seasonal water use and basal area, DBH, and sapwood basal area. Young stands have a greater sapwood area per unit basal area, as well as a greater sap flux density, resulting in greater water use by the stand, than a mature stand with the same area. Water use by the trees linearly decreases as the number of trees decreases. Additionally, water use decreases as the canopy closes up, and suppressed trees die out, lowering stand density (Stubblefield et al., 2012). According to sap flow measurements conducted in western Oregon, young Douglas-fir stands had 3.27 times higher water usage than old-growth stands during summer months (Moore et al., 2004). This period coincides with the dry season in the Tenmile Creek basin when water resources are in high

demand by humans. These factors are especially relevant in this region because of historic timber harvesting that has resulted in the regrowth of dense stands of even-aged young Douglas firs. These stands have not undergone the stem exclusion stage and will continue to use high amounts of water until this occurs. In the past, Indigenous land practices such as intentional burns were used to weed out dense young trees, but these have not been practiced since colonization. Stubblefield et al. (2012) used stand growth modeling to determine that stands in the nearby Mattole River basin would use less water as the number of young trees (<5 cm diameter) die off due to canopy enclosure and stem suppression.

Fire Regime

These factors are especially relevant in this region because of historic timber harvesting that has resulted in the regrowth of dense stands of even-aged young Douglas firs. These stands have not undergone the stem exclusion stage and will continue to use high amounts of water until this occurs. Since European colonization, fire suppression has become the primary forest management technique. The composition of the forest has changed considerably since it was a managed old-growth forest. It is predicted that extended periods without fire activity increase the probability of shrubs being taken over by conifers. Additionally, the buildup of understory shade-tolerant plants can create fuel ladders that can spread the fire from ground level into the tree canopy, increasing the likelihood of tree death (Perry et al., 2011).

Fire regimes are a metric of the timing and intensity of fires that occur over long-term scales—this gradient of fire intensity that is measured by the mortality it inflicts on a stand. A low severity regime is considered one where less than 20% of the basal area or overstory trees are eliminated per fire. These fires reduce the volume of the most flammable fuels but have minimal impacts on stand mortality, but happen more frequently. High severity fire regime is one where 70% of the basal area or overstory trees are eliminated. This high severity regime kills the most trees in instances of crown fires, where the fire moves from the ground up a fuel ladder to ignite the crown foliage of the tree. Between these two extremes is a mixed-severity regime (Perry et al., 2011). In the past, Indigenous land practices such as intentional burns were used to weed out dense young trees and understory vegetation. This burning has played a large role in shaping the landscape since human occupation. It is thought that these practices modified the fire regime of the areas throughout the Northwest. By introducing fire consistently, the regime is thought to have changed from a mixed-severity to low-severity. Fire creates more variation within forest structure, which opens up the possibility for a greater number of habitats (Safford & Van de Water, 2014) (Jain et al., 2012). Additionally, it increases the edge effect, or the gradient, between ecosystems, increasing biodiversity, and ecosystem resilience. Modern fire suppression approaches have increased the density of trees and undergrowth, directly impacts low flow events by increasing water demand. There is also an increase in conditions that favor crown fires, which are associated with higher tree mortality and burn severity (Perry et al., 2011). This could be especially troublesome, considering that there have been abnormal outbreaks of pathogens that can decimate forests. In Northern California, Sudden Oak Death targets Tanoak, decreasing their populations and changing mixed forest to conifer dominated forests. Additional pathogens that can alter the species make up of forest include the mountain pine beetle and the pine engraver beetle (Jain et al., 2012). Increased rate of pathogens will

be especially impactful to regions of dense homogeneous forests that are less resilient to disturbance, creating vast areas of tree mortality. Dead trees and diseased trees pose an increase in the severe fire risk for nearby human settlements.

In addition to changes in biological conditions, there are impacts to the soil as well. Fire suppression causes the organic matter to accumulate both above and below ground, altering the soil composition. As the soil's organic matter is burned off, it decreases the water holding capacity of the leading to increased surface runoff (Jain et al., 2012).

Elder Creek Streamflow

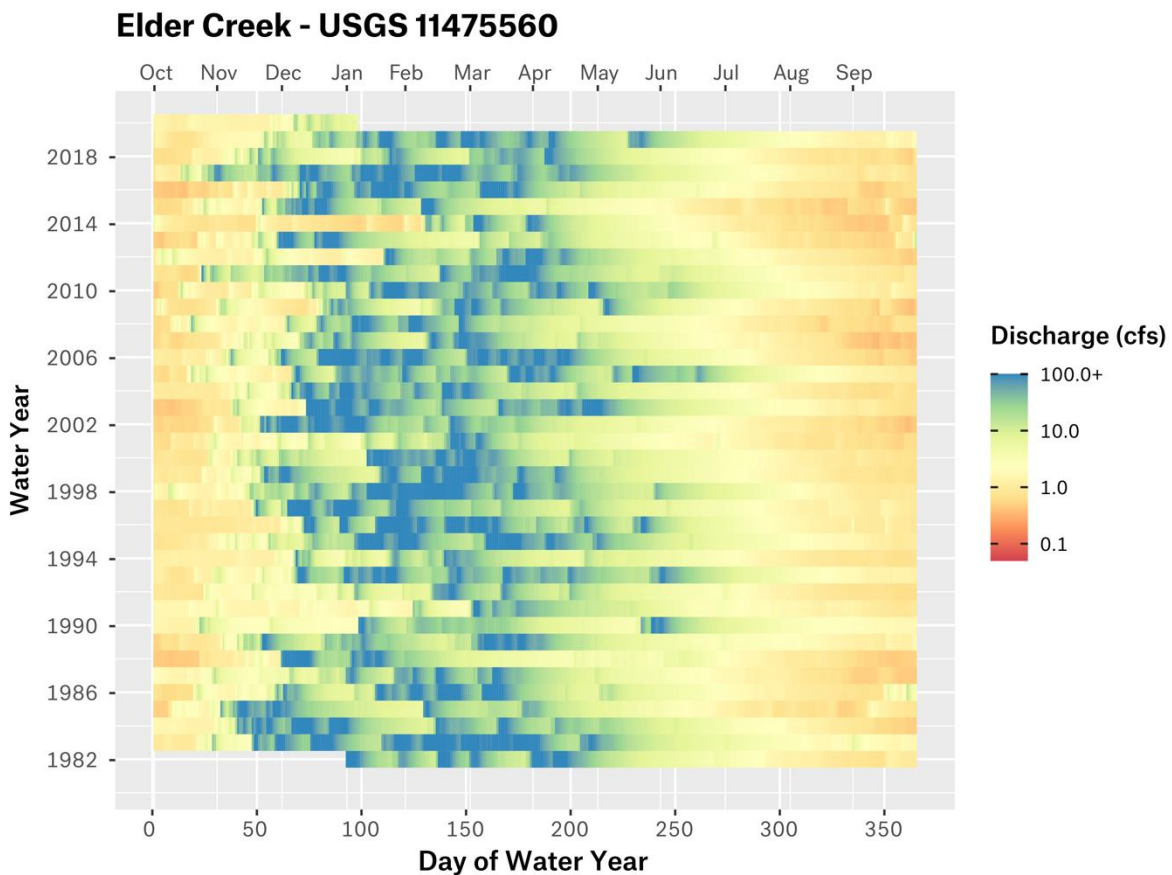


Figure 14. Raster plot of Elder Creek (USGS 11475560) streamflow from 1 Jan 1982 – 31 Dec 2019 on a logarithmic scale.

Elder Creek maintains its flow the entire year and also does not trend to extreme low flows, placing less pressure on biological systems that depend on streamflow during the dry season. The robust annual streamflow is due to a combination of geology, forest conditions, and lack of human disturbance.

Methods

Drainage Area Ratio

To estimate runoff in small (<30 mi²) ungauged catchments on the north coast, the California State Water Resources Control Board (SWRCB) uses a simple method utilizing ratios of drainage area and precipitation in a gauged reference basin and an ungauged basin of interest (Mann et al., 2004). Flow transfer methods of this type are best used for estimating flows of a sub-basin within a larger drainage basin, but SWRCB has used it in different drainage basins that are in close proximity (Mann et al., 2004). The method assumes that the basins being compared have similar hydrologic response characteristics and that streamflow is the same per unit area in both basins (Mann et al., 2004).

Equation 1. SWRCB Drainage Area Ratio equation

$$Q_u = Q_g \times \left(\frac{A_u}{A_g} \right) \times \left(\frac{P_u}{P_g} \right)$$

The drainage-area ratio equation (DAR) used by SWRCB is shown by Equation 1, where Q_u is daily mean streamflow in the ungauged basin, Q_g is daily mean streamflow in the gauged basin, A_u is the drainage area in the ungauged basin, A_g is the drainage area in the gauged basin, P_u is the annual precipitation in the ungauged basin, and P_g is the annual precipitation in the gauged basin (Mann et al., 2004).

Our calculations use daily mean streamflow values from nearby Elder Creek (USGS 11475560) acquired using the *dataRetrieval* package for R (Laura DeCicco et al., 2020). We used 30-year (1981–2010) normal annual precipitation values from the PRISM dataset, using the values from the 4 km grid cell containing the centroid point of each drainage basin to ensure that quantities were representative for the entire watershed of interest (Table 7; Oregon State University, 2020). These values reflect a mild rain shadow effect in the watersheds east of the regional drainage divide.

Table 7. Parameters used in drainage area ratio calculations

| Watershed | Drainage Area (mi²) | Annual Precipitation (in) |
|------------------|---------------------------------------|----------------------------------|
| Elder Creek | 6.47 | 89.57 |
| BRL | 2.98 | 73.78 |
| SCL | 4.85 | 70.60 |

Using Equation 1, we calculated historic and contemporary unimpaired daily streamflow in BRL and SCL for 38 years (1982–2019). Because of the substantial differences in bedrock geology and critical zone architecture highlighted earlier in this document, estimations of naturalized streamflow using DAR for BRL and SCL are limited. Additionally, any errors in the rating curves at the reference basin or the basin of study will introduce hidden errors in the resulting modeled flow.

VELMA

In order to estimate unimpaired streamflow in BRL and SCL in more detail than is possible with DAR, we used the Visualizing Ecosystem Land Management Assessments (VELMA) model. VELMA is a spatially distributed ecohydrologic model developed at the U.S. Environmental Protection Agency that is capable of simulating runoff, nutrient cycling, and evapotranspiration under different land management conditions (Abdelnour et al., 2011; McKane et al., 2014). Like other physically-based distributed models, VELMA requires a large number of data inputs, requiring the user to collect data from many sources and make estimates where data is unavailable (Sitterson et al., 2017). Examples of some of VELMA’s data requirements and the sources used in this study are listed in Table 8. The VELMA model simulations are calculated by calendar year (January-Dec) instead of water year (October-September).

Table 8. Some required VELMA data inputs and sources used

| Data Input | Format | Source |
|---------------------------|---------------|--|
| Digital elevation model | Spatial | USGS 3DEP |
| Land cover classification | Spatial | NLCD (Homer et al., 2020) |
| Soil type classification | Spatial | NRCS gNATSGO (Soil Survey Staff, 2019) |
| Cover age | Spatial | LandTrendr (Kennedy et al., 2010) |
| Daily precipitation | Tabular | PRISM (Oregon State University, 2020) |
| Daily mean temperature | Tabular | PRISM |
| Observed streamflow | Tabular | USGS NWIS |
| Soil physical properties | Discrete | Calibrated; (Dingman, 2015) |
| Land cover properties | Discrete | Calibrated; Various sources |

Our models for each watershed were based on a 10 m x 10 m grid. We used elevation data from the USGS 3D Elevation Program (3DEP) that were “flat-processed” as recommended by VELMA developers to facilitate stream network routing (McKane et al., 2014). Spatial data from other sources (e.g., gNATSGO, LandTrendr, NLCD) were not consistently available at an identical resolution and were resampled to fit the elevation data. Tabular climate data inputs (e.g., daily precipitation, mean temperature) were acquired from PRISM, using the Explorer tool to query interpolated values from the centroid of each drainage basin (Oregon State University, 2020). Discrete data inputs (e.g., soil physical properties, land cover properties) came from a wide variety of sources and VELMA defaults were used where other data was unavailable (McKane et al., 2014). Many of these discrete inputs—especially soil properties—were calibrated for the final model runs.

We calibrated our regional VELMA model using data from Elder Creek due to its geographic proximity to the basins of interest, long stream gauge record, and intensive study of the area by researchers at the University of California Angelo Reserve (Dralle et al., 2018; Hahm et al., 2019; Salve et al., 2012). Following this regional calibration, we used VELMA to simulate historical and unimpaired streamflow in BRL and SCL. Simulations in each watershed were completed for all calendar years in which PRISM climatic data was available at the time (Elder Creek: 1981-2018; BRL and SCL: 1982-2019).

We evaluated the output of VELMA model runs for calibration using a stratified and iterative procedure, using the Nash-Sutcliffe Efficiency (NSE) as the primary indicator of goodness-of-fit (Equation 2). NSE is a commonly used index in hydrologic modeling that ranges from $-\infty$ to 1, where a value equal to 1 indicates a perfect model fit and a value equal to 0 indicates that modeled values are as accurate as the mean of observed values (Nash and Sutcliffe, 1970). Additionally, we calculated NSE with log-transformed streamflow (logNSE) to gauge model performance for low flows (Oudin et al., 2006).

Equation 2. Nash-Sutcliffe Efficiency equation. \bar{O} is the mean of the observed values, $S.D.$ represents the standard deviation of the observations, O_i is the original value, and P_i represents the sample (of size N) containing the observations and the model estimates.

$$NSE = 1 - \frac{\sum_{i=1}^N (O_i - P_i)^2}{\sum_{i=1}^N (O_i - \bar{O})^2} = 1 - \left(\frac{RMSE}{SD} \right)^2$$

At the start of calibration, we ran VELMA for the first 4 model years (1981-1984) and evaluated modeled streamflow using NSE and logNSE on an annual and cumulative basis. VELMA simulations are calculated by calendar year (January-Dec)—annual goodness-of-fit metrics are also calculated by calendar year. When chosen parameters resulted in both the median annual NSE and cumulative NSE meeting our goodness-of-fit threshold (0.6) and logNSE remained high (0.8-0.9), we ran all 38 model years (1981-2018) and evaluated annual and cumulative NSE, as well as logNSE. The iterative nature of this procedure is inherently time-consuming when calibrating the model manually. We instead used a version of VELMA that is coupled with a multi-objective evolutionary algorithm (MOEA-VELMA) to automate parameter calibration in an unsupervised environment (Hoghooghi et al., 2018).

Deficit Calculations

There are many methods proposed in the literature for establishing environmental flows in streams that are regulated or have water diverted from them (Kendy et al., 2012). In this report, we take a hydrological “percent-of-flow” approach assessing the magnitude of dry season streamflow in BRL and SCL (Richter et al., 2012). We calculate a 10% and 20% reduction in daily VELMA-modeled streamflow—where a reduction $\leq 10\%$ is considered ecologically protective and a reduction greater than 20% may cause significant harm (Richter et al., 2012). Observed daily streamflow values from BRL and SCL were then subtracted from the “reduced” flows to assess the surface water deficit under each diversion scenario. To account for the inherent difficulty in recording extremely low streamflow, only deficits greater than 0.05 cfs were included in our calculations. Additionally, we calculated deficits as a percentage of seasonal streamflow yield to analyze total season water deficits.

Simulated Historic Conditions

Using the calibrated VELMA models for BRL and SCL, we made modified two of the spatial inputs (cover classification and tree age) to estimate the rainfall-runoff behavior before significant land-use changes occurred in the catchments. We modeled this change as a 30% reduction in conifer forest density, where the interstitial spaces are occupied by grasses or shrubs, and a substantial increase in tree age in a 25%

portion of the forest. Due to the paucity of historical land cover data, this model is cursory and assumptions are not intended to be historically accurate.

Alterations were made only to cells previously classified as “conifer forest.” A subset of these cells was selected for “thinning,” generated by randomly selecting 30% of all conifer cells. An additional subset was selected for “aging,” generated by randomly selecting 25% of the remaining conifer cells.

The thinning subset was used as a masking layer to set values in the tree age raster file to 0, and additionally subset using a 30%/70% random selection to reclassify the cover classification raster as “shrub” and “grass,” respectively.

The aging subset of cells had their values reassigned to whole numbers between 100 and 400 using a random number generator. These values were then added to corresponding cell values in the tree age raster. Table 9 shows the relative land cover abundances before and after we applied the historical conditions model.

Table 9. Simulated old-growth spatial statistics in Big Rock Cr. and Streeter Cr.

| Watershed | Cover Class | Current Conditions | | Simulated Old Growth | |
|------------------|--------------------|---------------------------|-----------------------|-----------------------------|-----------------------|
| | | # of cells | % of catchment | # of cells | % of catchment |
| BRL | Conifer | 41972 | 53.9% | 29570 | 38.0% |
| | Grass | 8799 | 11.3% | 18005 | 23.1% |
| | Hardwood | 4651 | 6.0% | 4651 | 6.0% |
| | Mixed Forest | 5162 | 6.6% | 5162 | 6.6% |
| | Shrub | 11586 | 14.9% | 14782 | 19.0% |
| | Bare Soil | 5645 | 7.3% | 5645 | 7.3% |
| SCL | Conifer | 72730 | 58.1% | 50992 | 40.7% |
| | Grass | 10477 | 8.4% | 25692 | 20.5% |
| | Hardwood | 10981 | 8.8% | 10981 | 8.8% |
| | Mixed Forest | 6214 | 5.0% | 6214 | 5.0% |
| | Shrub | 15375 | 12.3% | 21898 | 17.5% |
| | Bare Soil | 9510 | 7.6% | 9510 | 7.6% |

Results

Drainage Area Ratio

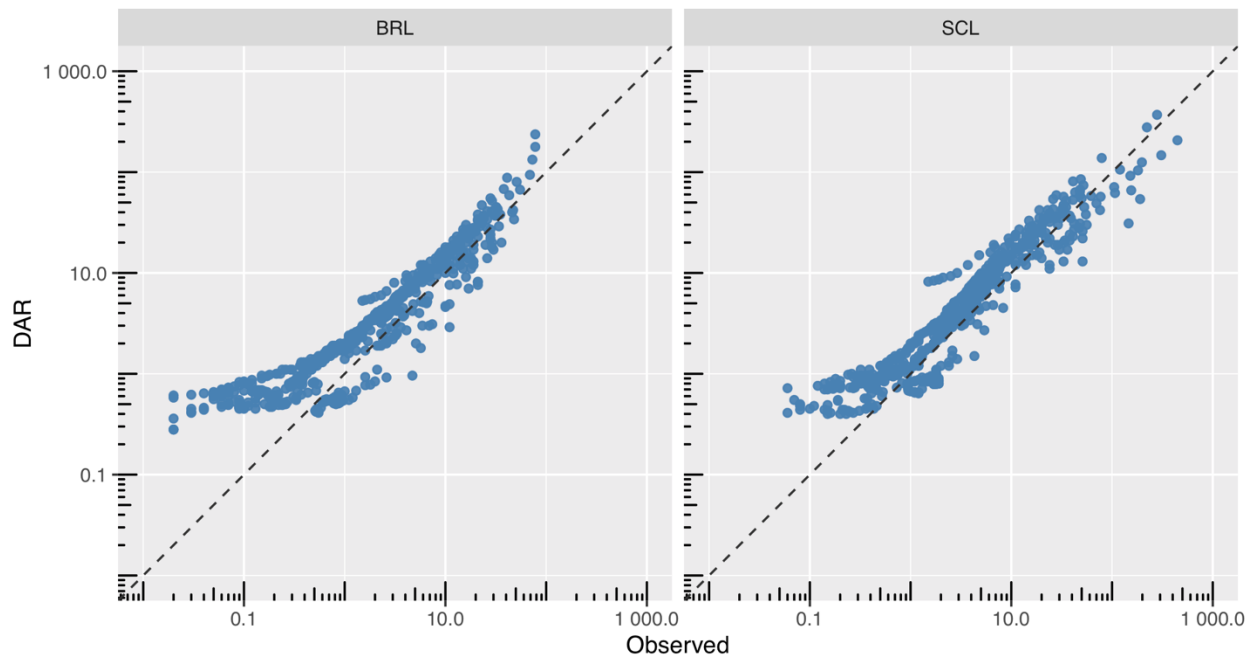


Figure 15. Quantile-quantile plot of modeled and observed streamflow values in Big Rock Creek and Streeter Creek. All values are in cubic feet per second.

Figure 155 shows quantile-quantile plots comparing daily mean streamflow (>0.01 cfs) observed at gauges and modeled using DAR for all records in 2018–2020. Values of daily streamflow calculated by DAR are generally larger than values observed at the gauging stations. As expected with watersheds in such close proximity, both BRL and SCL show linearity with DAR values through a large part of the gauging record. However, both DAR streamflow values are positively biased and show a strong curvilinear relationship at values <1.0 cfs. Departures in linearity may suggest that the rainfall-runoff processes in the reference watershed differ from those in BRL and SCL. For values <0.1 cfs, the median percent difference was 180% in BRL and 94.9% in SCL. The median percent difference between DAR and observed values >1.0 cfs was 44.3% in BRL and 21.7% in SCL. These values indicate that values modeled by DAR are generally overestimated for the entire flow record.

VELMA

Elder Creek Calibration

Following calibration of VELMA using Elder Creek, our selected model parameters resulted in metric values that exceeded our thresholds for model fit: annual median NSE = 0.67, cumulative NSE = 0.79, cumulative logNSE = 0.93. Over the 38-year model run, 15 years scored below the threshold NSE value

and 2 years (1985 and 1990) had negative NSE values.

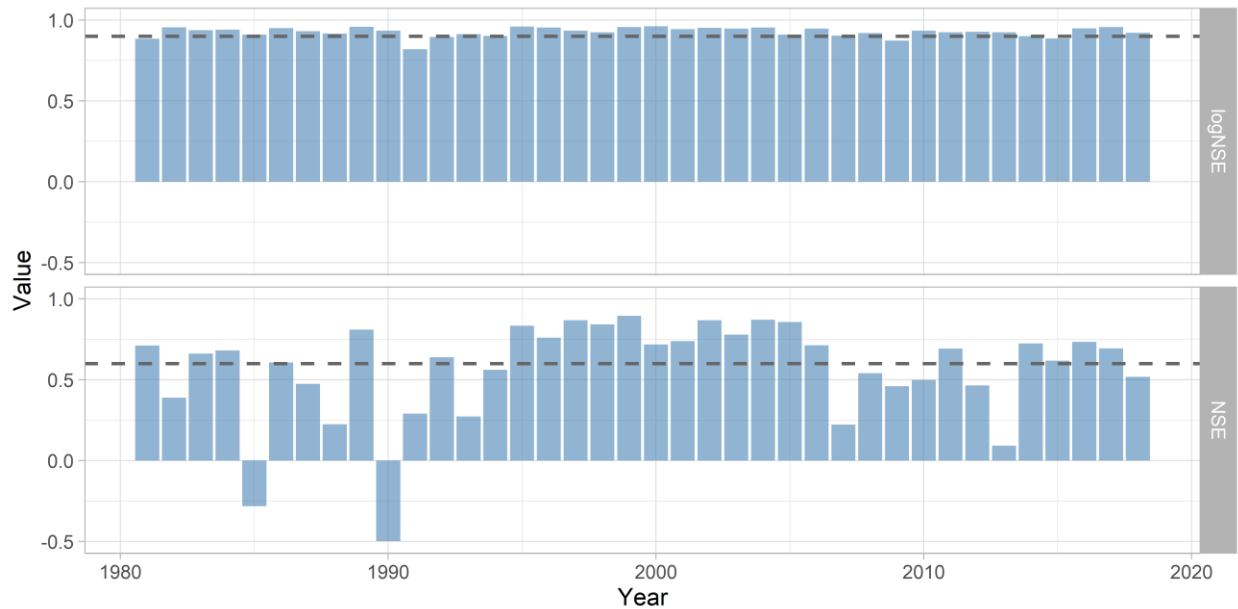


Figure 16. Goodness-of-fit metrics from final Elder Creek VELMA calibration. Dashed lines represent threshold values ($\logNSE = 0.9$; $NSE = 0.6$).

Inspection of model results on a finer temporal scale reveals some areas in which the model did not perform well. Figure 17 shows a daily hydrograph comparing observed discharge with modeled discharge for the 2018 recession limb (2018 $NSE = 0.52$). VELMA simulates a smooth recession limb until the first significant rainfall—in 2018, this resulted in periods of overestimation and underestimation of discharge. Exaggerated peak discharges occur with precipitation events surrounding a streamflow recession. We hypothesize that this may occur because VELMA calculates the water balance on a daily timestep and is unable to account for the intensity of rainfall. An additional cause of exaggerated peaks may be due to using modeled climatic data (PRISM) in the absence of weather monitoring in the basins.

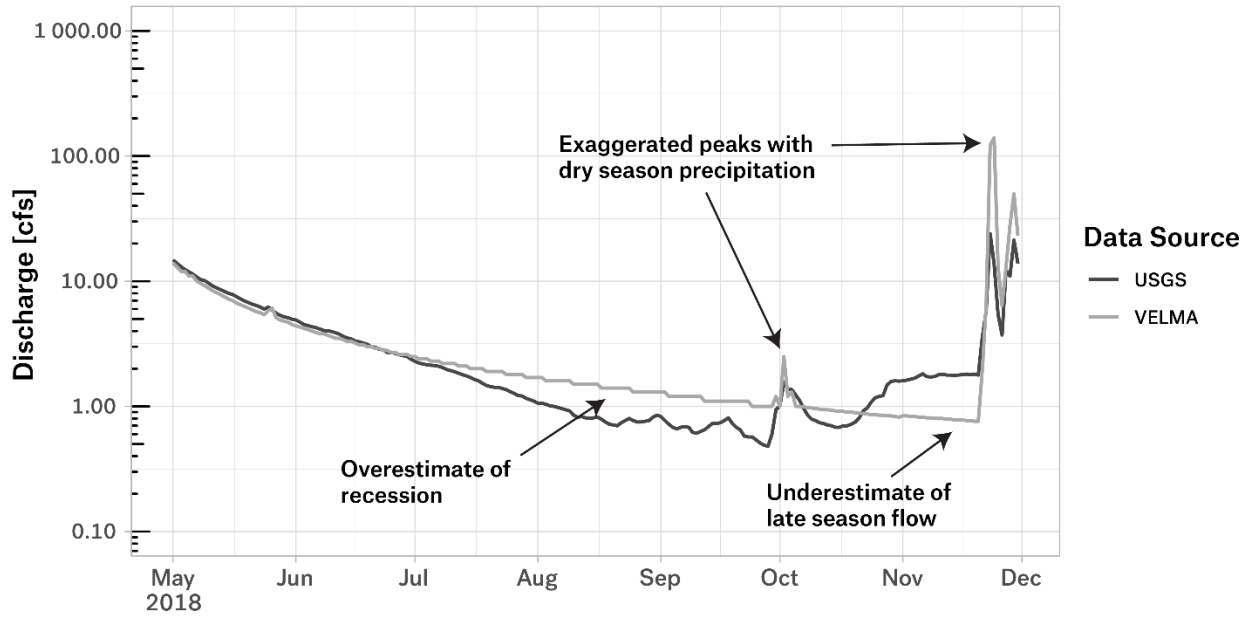


Figure 17. Comparison of modeled and gauged summer recession limb streamflow in Elder Creek, 2018.

Big Rock Creek and Streeter Creek

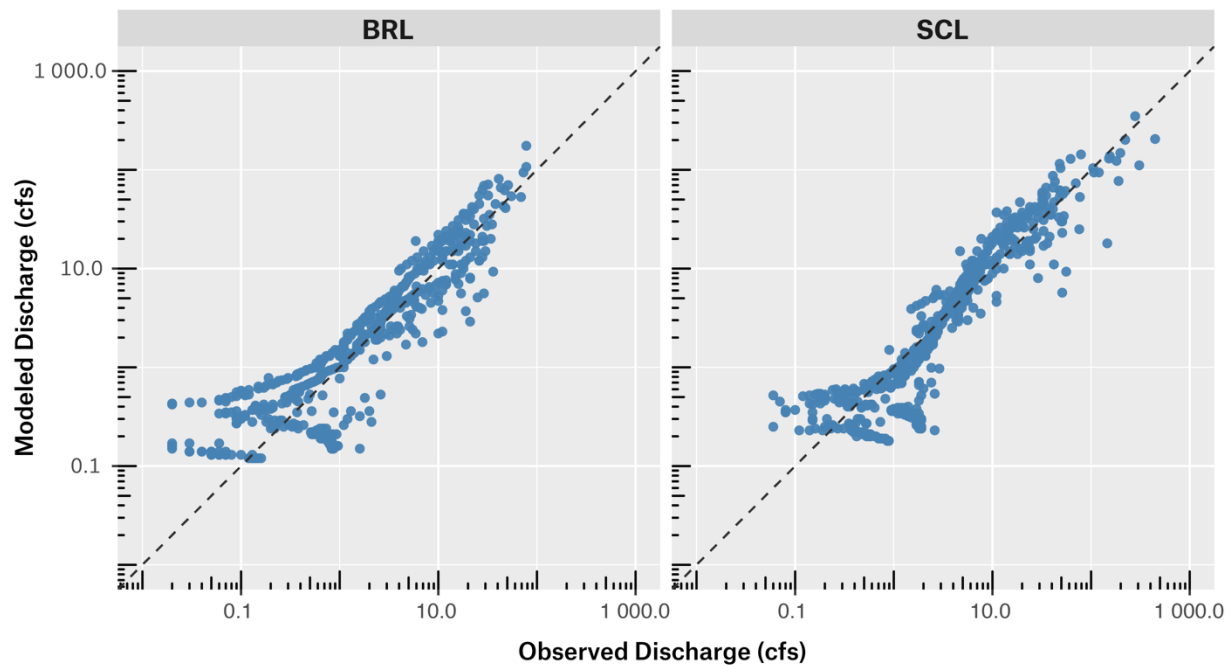


Figure 18. Quantile-quantile plot of modeled and observed discharges in Big Rock and Streeter Creek using VELMA. The dashed line represents a 1:1 ratio between modeled and observed values.

VELMA simulated streamflow values in BRL and SCL are similar to simulated values from DAR, with some distinct differences (Figure 18). Both methods produced pronounced left tails, indicating that estimated low flows are of greater magnitude than observed values. VELMA shows a greater variation in these values than DAR. BRL shows a positive bias for values above 1.0 cfs, similar to the bias seen in the DAR

Big Rock and Streeter Creeks Base Flow Analysis

model for SCL. SCL shows positive bias for flows greater than 4.0 cfs, but some negative bias for flows between 1.0 cfs and 4.0 cfs. Overall, there is more variation in VELMA modeled flows than DAR, but model fit at moderate to high flows is good.

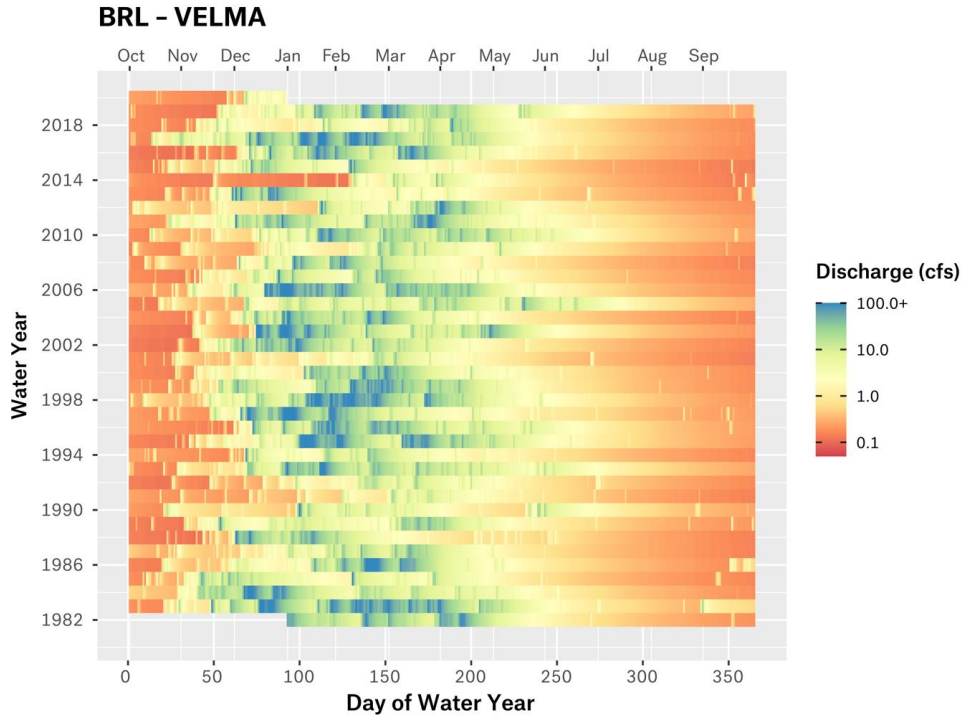


Figure 19. Raster plot for VELMA modeled streamflow in Big Rock Creek.

In raster hydrographs, streamflow recessions are seen as smooth gradients and late season discharge is very low—a behavior also observed in the Elder Creek calibration results (Figure 19; Figure 20). Drought years (e.g., 1991, 2001, and 2014) have very low volumes of discharge, but neither BRL nor SCL have periods of zero flow.

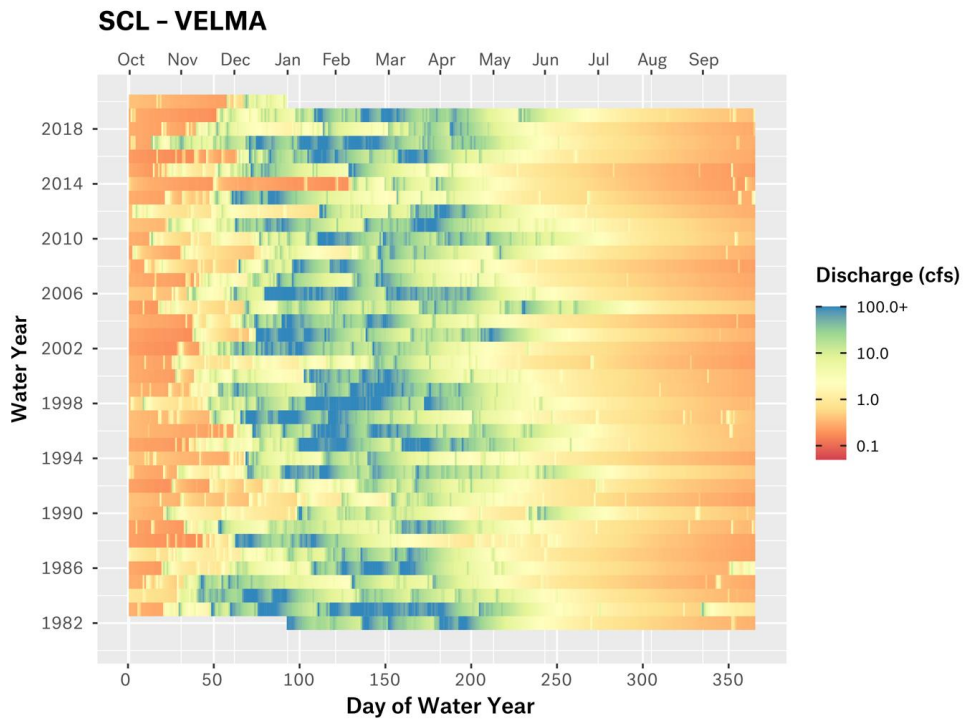


Figure 20. Raster plot of VELMA modeled streamflow in Streeter Creek.

Summer Streamflow Deficits

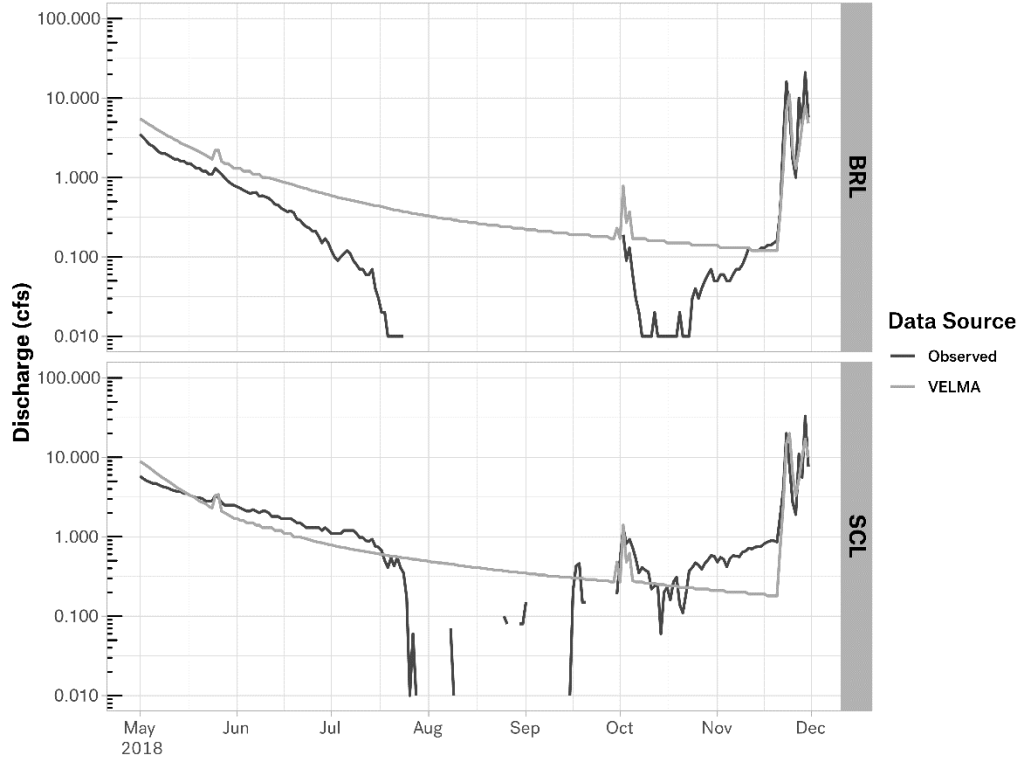


Figure 21. Summer 2018 recession hydrographs of BRL and SCL, comparing observed and modeled values

Streamflow monitoring in BRL and SCL began on 26 April 2018. By the end of July 2018, both creeks ceased to have measurable surface water flow (Figure 21). Steady flow did not return until early October, and flow was intermittent in BRL until late October 2018. VELMA models for this period showed a continuous recession, with the lowest flows around 0.10-0.20 cfs. The observed hydrograph for SCL was larger in magnitude from late October through mid-November, possibly the result of debris blocking the outlet of the gauging pool.

Observed streamflow in May-October 2019 did not recede as quickly as the previous year, nor were there any periods of immeasurably low discharge (Figure 22). Modeled values are in good agreement with observed streamflow values through early July in BRL and early August in SCL, at which time observed values negatively depart from the model. Minimum flows in both creeks occurred in late August (BRL = 0.06 cfs; SCL = 0.12 cfs) and were significantly lower than VELMA streamflow values on this date (BRL = 0.34 cfs; SCL = 0.50 cfs).

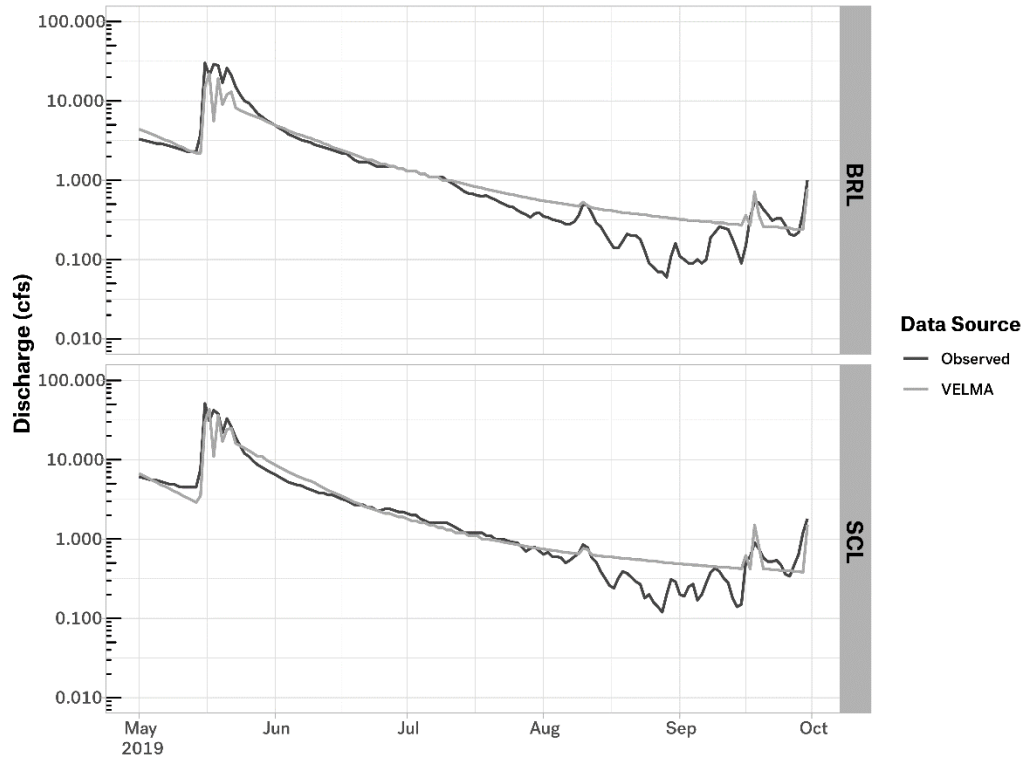


Figure 22. Summer 2019 recession hydrographs of BRL and SCL, comparing observed and modeled values

The summer season deficits in BRL and SCL in 2018 are significant—the observed yield in BRL was 50.9% (60.93 million gal.) less than the unimpaired yield modeled with VELMA and the yield in SCL was 12.9% (23.10 million gal.) less than unimpaired yield (Table 10). In 2019, BRL observed yield was higher than VELMA yield and SCL yield was 7.1% (16.21 million gal.) short of the unimpaired value.

Table 10. Summer season water deficits in Big Rock Cr. and Streeter Cr.

| Watershed | Source | Summer 2018 ¹ | | | Summer 2019 ² | | |
|-----------|----------|--------------------------|----------------------|------------|--------------------------|----------------------|------------|
| | | Yield | Deficit ³ | Percentage | Yield | Deficit ³ | Percentage |
| BRL | Observed | 58.72 | – | – | 154.19 | – | – |
| | VELMA | 119.65 | 60.93 | 50.9% | 139.00 | – | – |
| SCL | Observed | 156.56 | – | – | 213.25 | – | – |
| | VELMA | 179.66 | 23.10 | 12.9% | 229.46 | 16.21 | 7.1% |

All yield and deficit values are in millions of gallons.

¹ 2018 summer deficits calculated from the beginning of the gauging record.

² 2019 summer deficits calculated after May peak streamflow.

³ Calculations extend until the first significant rainfall after the summer recession.

Figure 23 shows the deficits in daily mean streamflow in BRL during the 2018 and 2019 summer recession. Nearly every day in summer 2018 showed a deficit between 0.1 cfs and 0.5 cfs compared to

the estimated unimpaired flow. Deficits during the same period in 2019 were shorter and less severe (0.1–0.25 cfs). Compared to estimated percent-of-flow diversions, the results were nearly identical in 2018 under a 10% diversion scenario. Under the 20% diversion scenario, deficits remained through the majority of the recession period, but were less severe. In 2019, deficits remained under both 10% and 20% diversion scenarios, but were significantly shorter and less severe (0.05–0.10 cfs) than 2018 values.

Figure 24 shows daily mean streamflow deficits in SCL during the 2018 and 2019 recession periods. The results in SCL generally match those in BRL, but the number of days with a streamflow shortage are fewer. Deficits are ≤ 0.5 cfs, except for two discrete periods (April-May 2018 and May-June 2019) when these deficits appear to be large. In both of these periods, VELMA calculated a rate of recession different than what was observed (Figure 21; Figure 22) and these deficits are likely artificially inflated. Under percent-of-flow diversions, deficits are only slightly reduced in magnitude and duration in 2018. In 2019, daily streamflow deficits remain under both scenarios but are ≤ 0.25 cfs. The remaining deficits under the 20% diversion scenarios suggest that streamflow in BRL and SCL is falling below ecologically protective volumes, even during years with normal precipitation.

Deficits under Percent-of-Flow Diversions

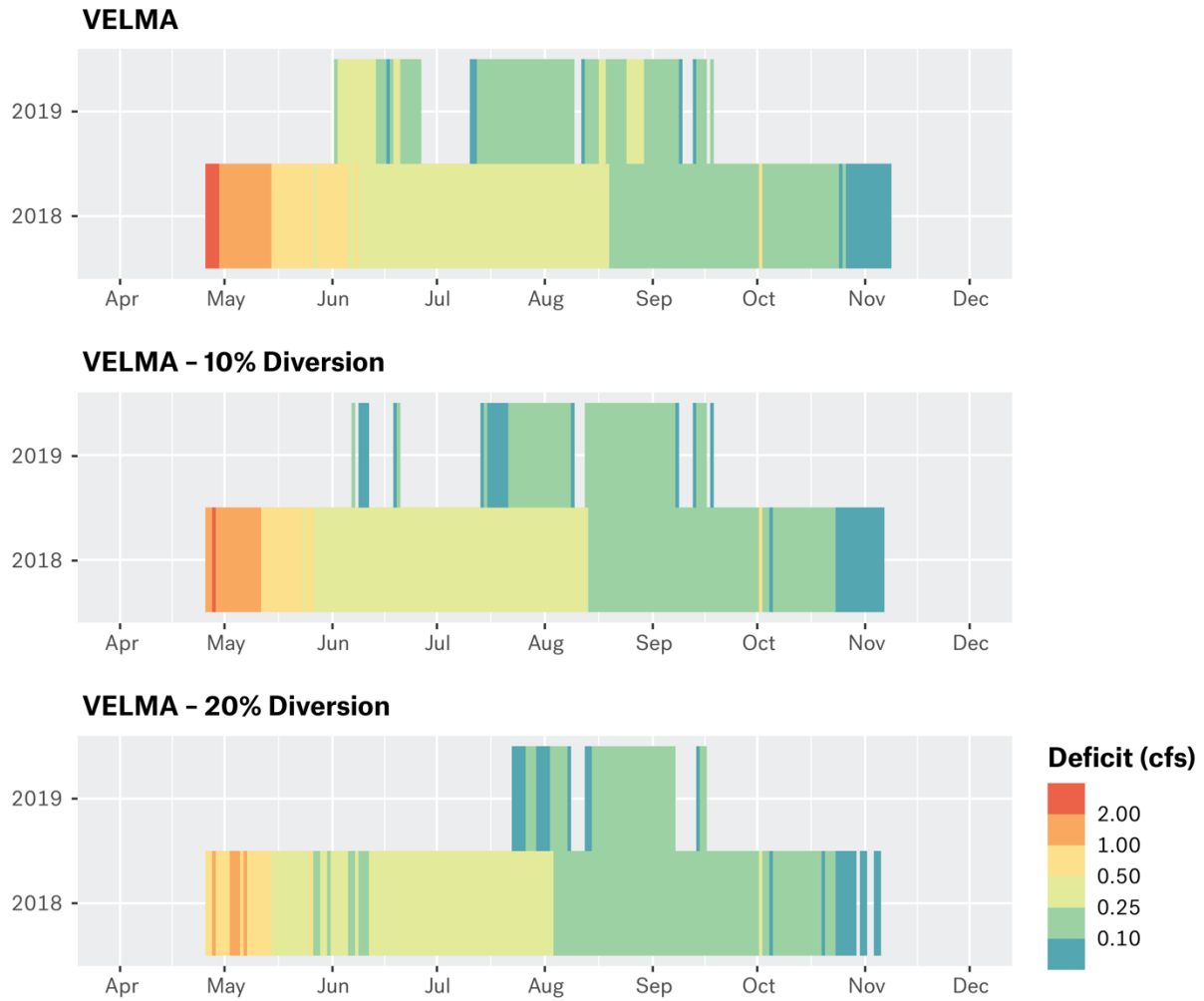


Figure 23. Daily streamflow deficits in Big Rock Creek as calculated under three baseline conditions: (1) VELMA modeled flow, (2) VELMA modeled flow with 10% subtracted, (3) VELMA modeled flow with 20% subtracted.

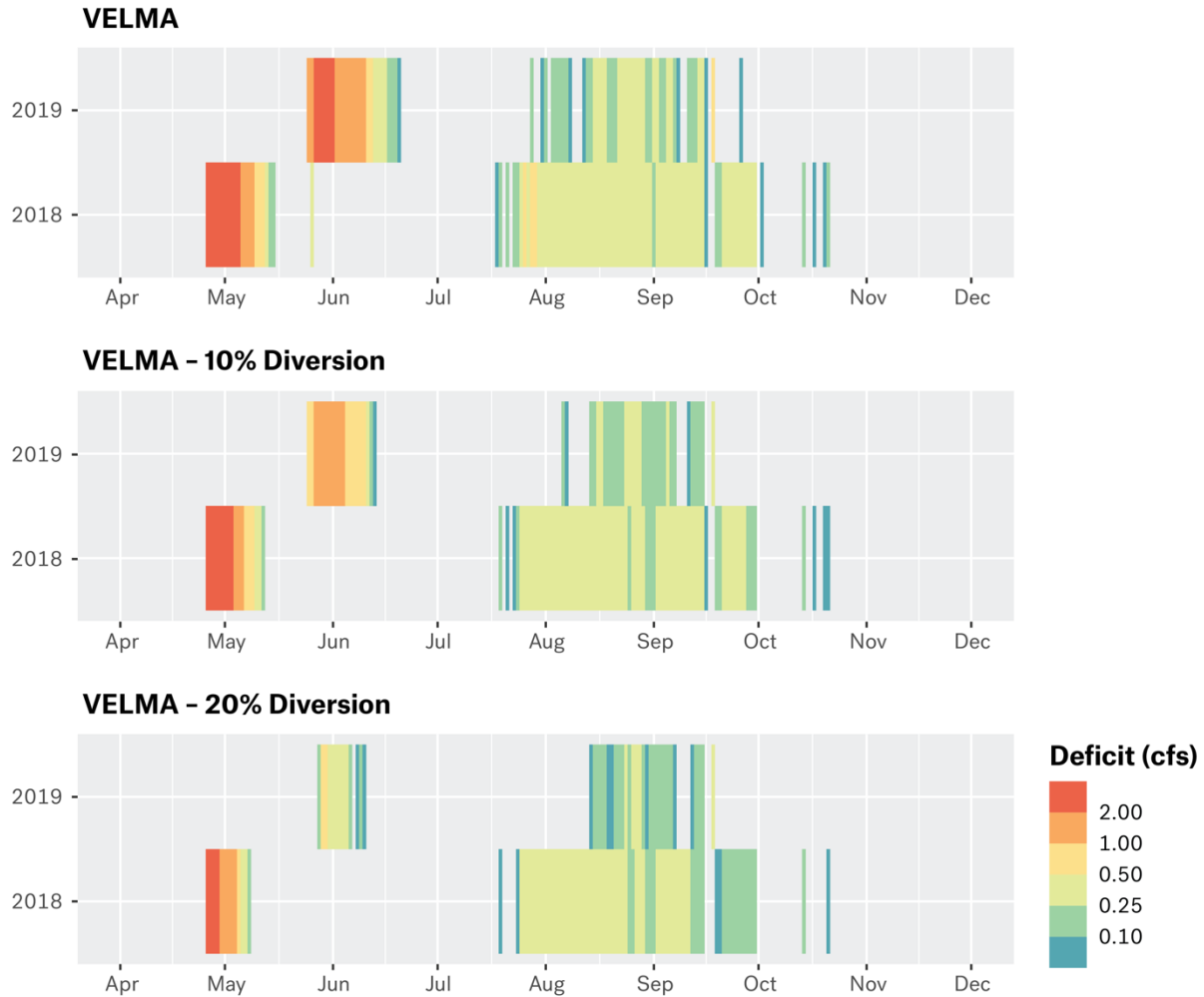


Figure 24. Daily streamflow deficits in Streeter Creek as calculated under three baseline conditions: (1) VELMA modeled flow, (2) VELMA modeled flow, (3) VELMA modeled flow with 10% subtracted, (4) VELMA modeled flow with 20% subtracted.

Historic Evapotranspiration

A modification of the land cover in the VELMA models for BRL and SCL by converting 30% of the coniferous forest to a mix of shrub and grassland and increasing the tree age in 25% of the cells resulted in an approximate 11% reduction in modeled evapotranspiration (Table 11). Eliminating mid-seral conifer from the modeled landscape reduced the soil water demand in the watersheds, allowing more precipitation to be transferred to the subsurface and end up as streamflow. Over the 38 years, the ratio between AET and precipitation decreased by approximately 0.05.

Table 11. Changes in modeled evapotranspiration (AET) with old-growth cover modifications

| Watershed | Period | Current Conditions | | Historic Conditions | |
|-----------|--------|--------------------|---------------|---------------------|---------------|
| | | AET (in/yr) | AET/P (in/in) | AET (in/yr) | AET/P (in/in) |
| BRL | 2018 | 28.98 | 0.636 | 25.93 | 0.569 |
| | 2019 | 30.49 | 0.472 | 26.86 | 0.416 |

| | | | | | |
|-----|------------|-------|-------|-------|-------|
| | 38-yr Mean | 30.07 | 0.498 | 26.63 | 0.441 |
| SCL | 2018 | 29.93 | 0.597 | 26.57 | 0.530 |
| | 2019 | 31.38 | 0.436 | 27.53 | 0.383 |
| | 38-yr Mean | 30.75 | 0.459 | 27.09 | 0.405 |

The reduction in evapotranspiration was translated into an average 9.3% increase in streamflow yield in BRL and a 7.9% increase in yield in SCL (Table 12). Increases are markedly higher in years with low flow—modeled streamflow yield increased by 15.5% (SCL) and 17.3% (SCL) in 2018. These results provide preliminary evidence that thinning of mid-seral trees has the potential to increase annual streamflow yields, particularly in years with low flows. Additional field-based measurements are necessary to validate these results, and several ongoing studies will provide insight into the efficacy of forest thinning on increasing base flows.

Table 12. Modeled yields in Big Rock Cr. and Streeter Cr. with old-growth cover modifications

| Watershed | Data Source | Current Condition Yield (million gal.) | Historic Condition Yield (million gal.) | Difference (million gal.) | Increase (%) |
|-----------|-------------|--|---|---------------------------|--------------|
| BRL | 2018 | 822.49 | 995.00 | 172.51 | 17.3% |
| | 2019 | 2159.73 | 2359.94 | 200.21 | 8.5% |
| | 38-yr mean | 1891.40 | 2085.56 | 194.16 | 9.3% |
| SCL | 2018 | 976.18 | 1155.46 | 179.28 | 15.5% |
| | 2019 | 2432.72 | 2625.31 | 192.59 | 7.3% |
| | 38-yr mean | 2153.39 | 2338.92 | 185.53 | 7.9% |

References

- Abdelnour, A., Stieglitz, M., Pan, F., McKane, R., 2011. Catchment hydrological responses to forest harvest amount and spatial pattern: CATCHMENT HYDROLOGICAL RESPONSE TO LAND USE. Water Resource. Res. 47. <https://doi.org/10.1029/2010WR010165>
- Asquith, W. H., Roussel, M. C., & Vrabel, J. (2006). Statewide Analysis of the Drainage-Area Ratio Method for 34 Streamflow Percentile Ranges in Texas (U.S. Geological Survey Scientific Investigations Report No. 2006–5268; p. 34).
- Bauer, S., Olson, J., Cockrill, A., van Hattem, M., Miller, L., Tauzer, M., & Leppig, G. (2015). Impacts of Surface Water Diversions for Marijuana Cultivation on Aquatic Habitat in Four Northwestern California Watersheds. PLOS ONE, 10(3), e0120016. <https://doi.org/10.1371/journal.pone.0120016>

- Berg, N., & Hall, A. (2015). Increased Interannual Precipitation Extremes over California under Climate Change. *Journal of Climate*, 28(16), 6324–6334. <https://doi.org/10.1175/JCLI-D-14-00624.1>
- Biondi, F., Gershunov, A., & Cayan, D. R. (2001). North Pacific Decadal Climate Variability since 166. *JOURNAL OF CLIMATE*, 14, 6.
- Butsic, V., & Brenner, J. C. (2016). Cannabis (*Cannabis sativa* or *C. indica*) agriculture and the environment: A systematic, spatially-explicit survey and potential impacts. *Environmental Research Letters*, 11(4), 044023. <https://doi.org/10.1088/1748-9326/11/4/044023>
- Cai, W., Borlace, S., Lengaigne, M., van Rensch, P., Collins, M., Vecchi, G., Timmermann, A., Santoso, A., McPhaden, M. J., Wu, L., England, M. H., Wang, G., Guilyardi, E., & Jin, F.-F. (2014a). Increasing frequency of extreme El Niño events due to greenhouse warming. *Nature Climate Change*, 4(2), 111–116. <https://doi.org/10.1038/nclimate2100>
- DeOreo, W. B. (2011). Analysis of water use in new single-family homes.
- Dingman, S.L., 2015. *Physical Hydrology*, 3rd ed. Waveland Press, Long Grove, IL.
- Dralle, D. N., Hahm, W. J., Rempe, D. M., Karst, N. J., Thompson, S. E., & Dietrich, W. E. (2018). Quantification of the seasonal hillslope water storage that does not drive streamflow: Catchment storage that does not drive streamflow. *Hydrological Processes*, 32(13), 1978–1992. <https://doi.org/10.1002/hyp.11627>
- Golden, H. E., Lane, C. R., Amatya, D. M., Bandilla, K. W., Raanan Kiperwas, H., Knightes, C. D., & Ssegane, H. (2014). Hydrologic connectivity between geographically isolated wetlands and surface water systems: A review of select modeling methods. *Environmental Modelling & Software*, 53, 190–206. <https://doi.org/10.1016/j.envsoft.2013.12.004>
- Hahm, W.J., Rempe, D.M., Dralle, D.N., Dawson, T.E., Lovill, S.M., Bryk, A.B., Bish, D.L., Schieber, J., Dietrich, W.E., 2019. Lithologically Controlled Subsurface Critical Zone Thickness and Water Storage Capacity Determine Regional Plant Community Composition. *Water Resour. Res.* 55, 3028–3055. <https://doi.org/10.1029/2018WR023760>
- Hoekstra, A. Y., & Chapagain, A. K. (2006). Water footprints of nations: Water use by people as a function of their consumption pattern. *Water Resources Management*, 21(1), 35–48. <https://doi.org/10.1007/s11269-006-9039-x>

- Hoghooghi, N., Golden, H., Bledsoe, B., Barnhart, B., Brookes, A., Djang, K., Halama, J., McKane, R., Nietch, C., Pettus, P., 2018. Cumulative Effects of Low Impact Development on Watershed Hydrology in a Mixed Land-Cover System. *Water* 10, 991. <https://doi.org/10.3390/w10080991>
- Homer, C., Dewitz, J., Jin, S., Xian, G., Costello, C., Danielson, P., Gass, L., Funk, M., Wickham, J., Stehman, S., Auch, R., Riitters, K., 2020. Conterminous United States land cover change patterns 2001–2016 from the 2016 National Land Cover Database. *ISPRS J. Photogramm. Remote Sens.* 162, 184–199. <https://doi.org/10.1016/j.isprsjprs.2020.02.019>
- Humboldt Growers Association. (2011). Humboldt County Growers Association (HGA) review of Humboldt County 314-55.1 Medical Marijuana Land uses.
- IPCC. (2018). Summary for Policymakers (Global Warming of 1.5°C. An IPCC Special Report on the Impacts of Global Warming of 1.5°C above Pre-Industrial Levels and Related Global Greenhouse Gas Emission Pathways, in the Context of Strengthening the Global Response to the Threat of Climate Change, Sustainable Development, and Efforts to Eradicate Poverty).
- Jain, T. B., Battaglia, M. A., Han, H.-S., Graham, R. T., Keyes, C. R., Fried, J. S., & Sandquist, J. E. (2012). A comprehensive guide to fuel management practices for dry mixed conifer forests in the northwestern United States (RMRS-GTR-292; p. RMRS-GTR-292). U.S. Department of Agriculture, Forest Service, Rocky Mountain Research Station. <https://doi.org/10.2737/RMRS-GTR-292>
- Jayko, A. S., Blake, Jr., M. C., McLaughlin, R. J., Ohlin, H. N., Ellen, S. D., & Kelsey, H. (1989). Reconnaissance Geologic Map of the Covelo 30- by 60-minute Quadrangle, Northern California [Map]. U.S. Geological Survey.
- Kendy, E., Apse, C., & Blann, K. (2012). *A Practical Guide to Environmental Flows for Policy and Planning*. The Nature Conservancy.
- Kennedy, R.E., Yang, Z., Cohen, W.B., 2010. Detecting trends in forest disturbance and recovery using yearly Landsat time series: 1. LandTrendr — Temporal segmentation algorithms. *Remote Sens. Environ.* 114, 2897–2910. <https://doi.org/10.1016/j.rse.2010.07.008>
- Książek, L., Woś, A., Florek, J., Wyrębek, M., Młyński, D., & Wałęga, A. (2019). Combined use of the hydraulic and hydrological methods to calculate the environmental flow: Wisłoka River, Poland: case study. *Environmental Monitoring and Assessment*, 191(4), 254. <https://doi.org/10.1007/s10661-019-7402-7>

- Laura DeCicco, Robert Hirsch, David Lorenz, David Watkins, 2020. Retrieval Functions for USGS and EPA Hydrologic and Water Quality Data. U.S. Geological Survey.
- Lovill, S. M., Hahm, W. J., & Dietrich, W. E. (2018). Drainage from the Critical Zone: Lithologic Controls on the Persistence and Spatial Extent of Wetted Channels during the Summer Dry Season. *Water Resources Research*, 54(8), 5702–5726. <https://doi.org/10.1029/2017WR021903>
- Mann, M.P., Rizzardo, J., Satowski, R., 2004. Evaluation of Methods Used for Estimating Selected Streamflow Statistics, and Flood Frequency and Magnitude, for Small Basins in North Coastal California (U.S. Geological Survey Scientific Investigations Report No. 2004–5068).
- McGregor, S., Timmermann, A., & Timm, O. (2010). A unified proxy for ENSO and PDO. Variability since 1650. *Clim. Past*, 17.
- McKane, R. B., Brookes, A., Djang, K., Stieglitz, M., Abdelnour, A. G., Pan, F., Halama, J. J., Pettus, P. B., & Phillips, D. L. (2014). VELMA Version 2.0 User Manual and Technical Documentation. U.S. Environmental Protection Agency.
- McKane, R.B., Brookes, A., Djang, K., Stieglitz, M., Abdelnour, A.G., Pan, F., Halama, J.J., Pettus, P.B., Phillips, D.L., 2014. VELMA Version 2.0 User Manual and Technical Documentation.
- McLaughlin, R. J., Ellen, S. D., Blake, Jr., M. C., Jayko, A. S., Irwin, W. P., Aalto, K. R., Carver, G. A., & Clarke, Jr., S. H. (2000). Geology of the Cape Mendocino, Eureka, Garberville, and Southwestern part of the Hayfork 30 x 60 Minute Quadrangles and Adjacent Offshore Area, Northern California (Miscellaneous Field Studies MF-2336). U.S. Geological Survey.
- Moore, G. W., Bond, B. J., Jones, J. A., Phillips, N., & Meinzer, F. C. (2004). Structural and compositional controls on transpiration in 40- and 450-year-old riparian forests in western Oregon, USA. *Tree Physiology*, 24(5), 481–491. <https://doi.org/10.1093/treephys/24.5.481>
- Moriasi, D. N., Arnold, J. G., Bingner, R. L., Harmel, R. D., Veith, T. L., & T. L. Veith. (2007). Model Evaluation Guidelines for Systematic Quantification of Accuracy in Watershed Simulations. *Transactions of the ASABE*, 50(3), 885–900. <https://doi.org/10.13031/2013.23153>
- Mount, J. (1995). California rivers and streams: The conflict between fluvial process and land use. University of California Press.
- Nash, J. E., & Sutcliffe, J. V. (1970). River flow forecasting through conceptual models part I — A discussion of principles. *Journal of Hydrology*, 10(3), 282–290. [https://doi.org/10.1016/0022-1694\(70\)90255-6](https://doi.org/10.1016/0022-1694(70)90255-6)

- Nash, J.E., Sutcliffe, J.V., 1970. River flow forecasting through conceptual models part I — A discussion of principles. *J. Hydrol.* 10, 282–290. [https://doi.org/10.1016/0022-1694\(70\)90255-6](https://doi.org/10.1016/0022-1694(70)90255-6)
- Oregon State University, 2020. PRISM Climate Group [WWW Document]. PRISM Clim. Group Or. State Univ. URL <http://prism.oregonstate.edu/> (accessed 11.13.19).
- Oudin, L., Andréassian, V., Mathevet, T., Perrin, C., Michel, C., 2006. Dynamic averaging of rainfall-runoff model simulations from complementary model parameterizations: DYNAMIC AVERAGING OF RAINFALL-RUNOFF MODELS. *Water Resour. Res.* 42. <https://doi.org/10.1029/2005WR004636>
- Perry, D. A., Hessburg, P. F., Skinner, C. N., Spies, T. A., Stephens, S. L., Taylor, A. H., Franklin, J. F., McComb, B., & Riegel, G. (2011). The ecology of mixed severity fire regimes in Washington, Oregon, and Northern California. *Forest Ecology and Management*, 262(5), 703–717. <https://doi.org/10.1016/j.foreco.2011.05.004>
- Pierce, D. W., Cayan, D. R., Das, T., Maurer, E. P., Miller, N. L., Bao, Y., Kanamitsu, M., Yoshimura, K., Snyder, M. A., Sloan, L. C., Franco, G., & Tyree, M. (2013). The Key Role of Heavy Precipitation Events in Climate Model Disagreements of Future Annual Precipitation Changes in California. *Journal of Climate*, 26(16), 5879–5896. <https://doi.org/10.1175/JCLI-D-12-00766.1>
- Queener, N., & Stubblefield, A. P. (2016). Spatial and Temporal Variability in Baseflow in the Mattole River Headwaters, California, USA. *Hydrology and Earth System Sciences Discussions*, 1–39. <https://doi.org/10.5194/hess-2016-300>
- R Core Team. (2017). R: A language and environment for statistical computing. R Foundation for Statistical Computing. <https://www.R-project.org/>
- Richter, B. D., Davis, M. M., Apse, C., & Konrad, C. (2012). A Presumptive Standard for Environmental Flow Protection. *River Research and Applications*, 28(8), 1312–1321. <https://doi.org/10.1002/rra.1511>
- Richter, B.D., Davis, M.M., Apse, C., Konrad, C., 2012. A Presumptive Standard for Environmental Flow Protection. *River Res. Appl.* 28, 1312–1321. <https://doi.org/10.1002/rra.1511>
- Richter, Brian D. (2009). Re-thinking environmental flows: From allocations and reserves to sustainability boundaries. *River Research and Applications*. <https://doi.org/10.1002/rra.1320>
- Safford, H. D., & Van de Water, K. M. (2014). Using fire return interval departure (FRID) analysis to map spatial and temporal changes in fire frequency on national forest lands in California (PSW-RP-

- 266; p. PSW-RP-266). U.S. Department of Agriculture, Forest Service, Pacific Southwest Research Station. <https://doi.org/10.2737/PSW-RP-266>
- Salve, R., Rempe, D.M., Dietrich, W.E., 2012. Rain, rock moisture dynamics, and the rapid response of perched groundwater in weathered, fractured argillite underlying a steep hillslope. *Water Resour. Res.* 48. <https://doi.org/10.1029/2012WR012583>
- Santoso, A., Mcphaden, M. J., & CAI, W. (2017). The Defining Characteristics of ENSO Extremes and the Strong 2015/2016 El Niño: ENSO Extremes. *Reviews of Geophysics*, 55(4), 1079–1129. <https://doi.org/10.1002/2017RG000560>
- Sitterson, J., Knightes, C., Parmar, R., Wolfe, K., Muche, M., Avant, B., 2017. An Overview of Rainfall-Runoff Model Types.
- Soil Survey Staff, 2019. Gridded National Soil Survey Geographic (gNATSGO) Database for California.
- Stubblefield, A., Kaufman, M., Blomstrom, G., & Rogers, J. (2012). Summer Water Use by Mixed-Age and Young Forest Stands, Mattole River, Northern California, USA (PSW-GTR-238; p. PSW-GTR-238). U.S. Department of Agriculture, Forest Service, Pacific Southwest Research Station. <https://doi.org/10.2737/PSW-GTR-238>
- Swain, D. L., Langenbrunner, B., Neelin, J. D., & Hall, A. (2018). Increasing precipitation volatility in twenty-first-century California. *Nature Climate Change*, 8(5), 427–433. <https://doi.org/10.1038/s41558-018-0140-y>
- Trenberth, Ke. (2011). Changes in precipitation with climate change. *Climate Research*, 47(1), 123–138. <https://doi.org/10.3354/cr00953>
- Trenberth, Kevin. (2016, January 4). What North America can expect from El Niño [The Conversation]. The Conversation. <https://theconversation.com/what-north-america-can-expect-from-el-nino-51959>
- Williams, L. (2001). Irrigation of wine grapes in California. *Practical Winery and Vineyard Journal*, December 2001.